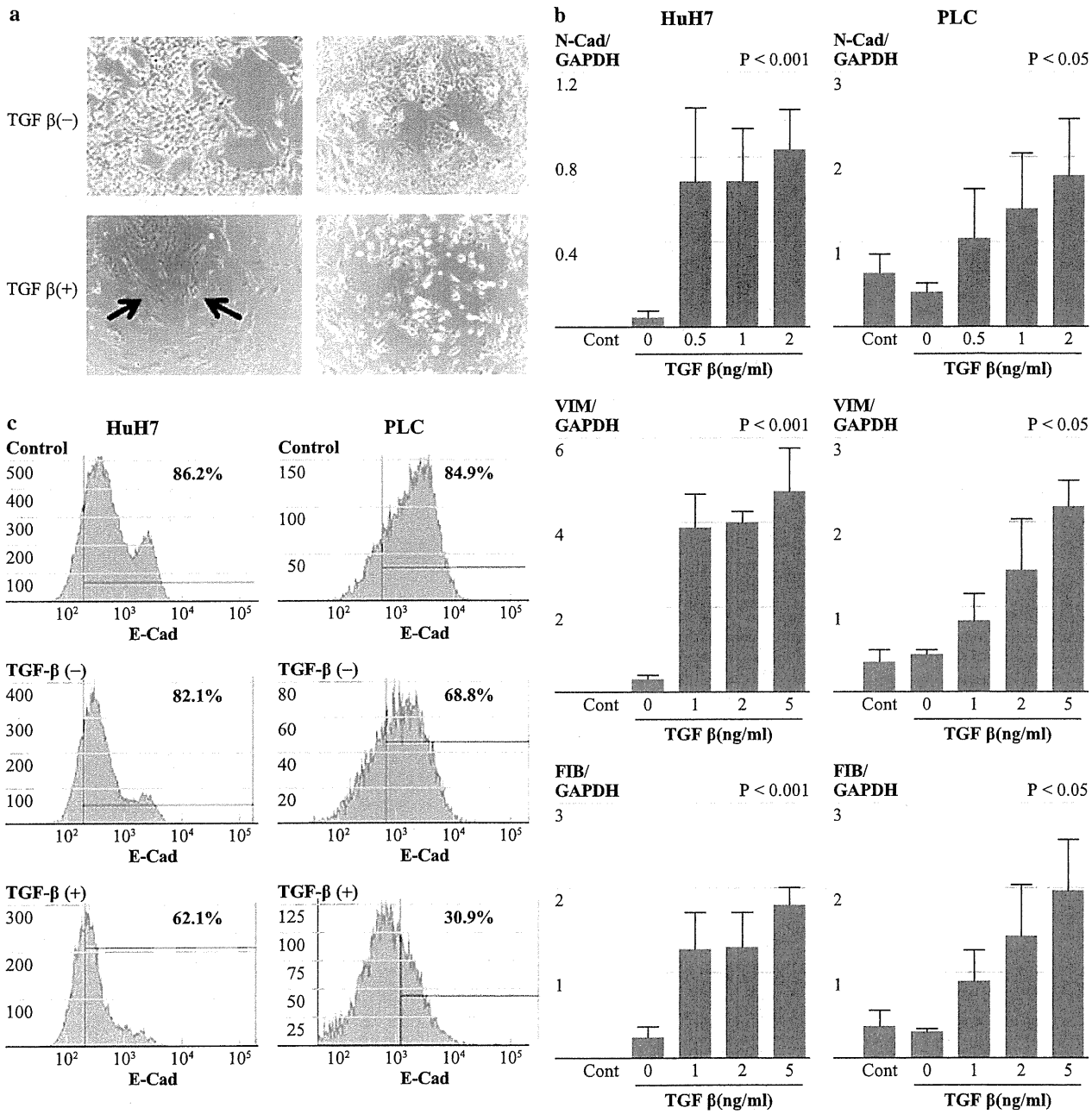

FIG. 1 TGF-β induces EMT in liver cancer cells. **a** Phase contrast microscopy of TGF-β treated (+) or untreated (−) cells of HuH7 and PLC/PRF/5 (PLC). The black arrow shows morphologically spindle-shaped cells. **b** Expression analysis of N-cadherin (N-cad), vimentin (VIM), and fibronectin (FIB) by qRT-PCR. GAPDH was used as internal control. **c** FACS analysis of E-cadherin with or without TGF-β treatment. Control: cells were cultured in conditional medium containing with 10% FBS. TGF-β: cells were treated with (+) or without (−) TGF-β in serum-free medium. HuH7 cells: treated with 1 ng/ml of TGF-β. PLC cells: treated with 2 ng/ml of TGF-β

from 2.5×10^3 cells, which indicated that $CD13^+$/N-cadherin$^+$ cells possess higher tumorigenic activity than $CD13^-$/N-cadherin$^-$ cells but lesser than that of $CD13^+$/N-cadherin$^-$ (Fig. 3c and d). The data are compatible with the results of the in vitro soft agar assay (Fig. 3a and b).

TGF-β Increased the ROS Level in N-cadherin$^+$ Liver Cancer Cells

It has been reported that the control of ROS is indispensable for hematopoietic stem cell maintenance.[31,32] In cancer, low ROS levels and radiation-resistance in breast

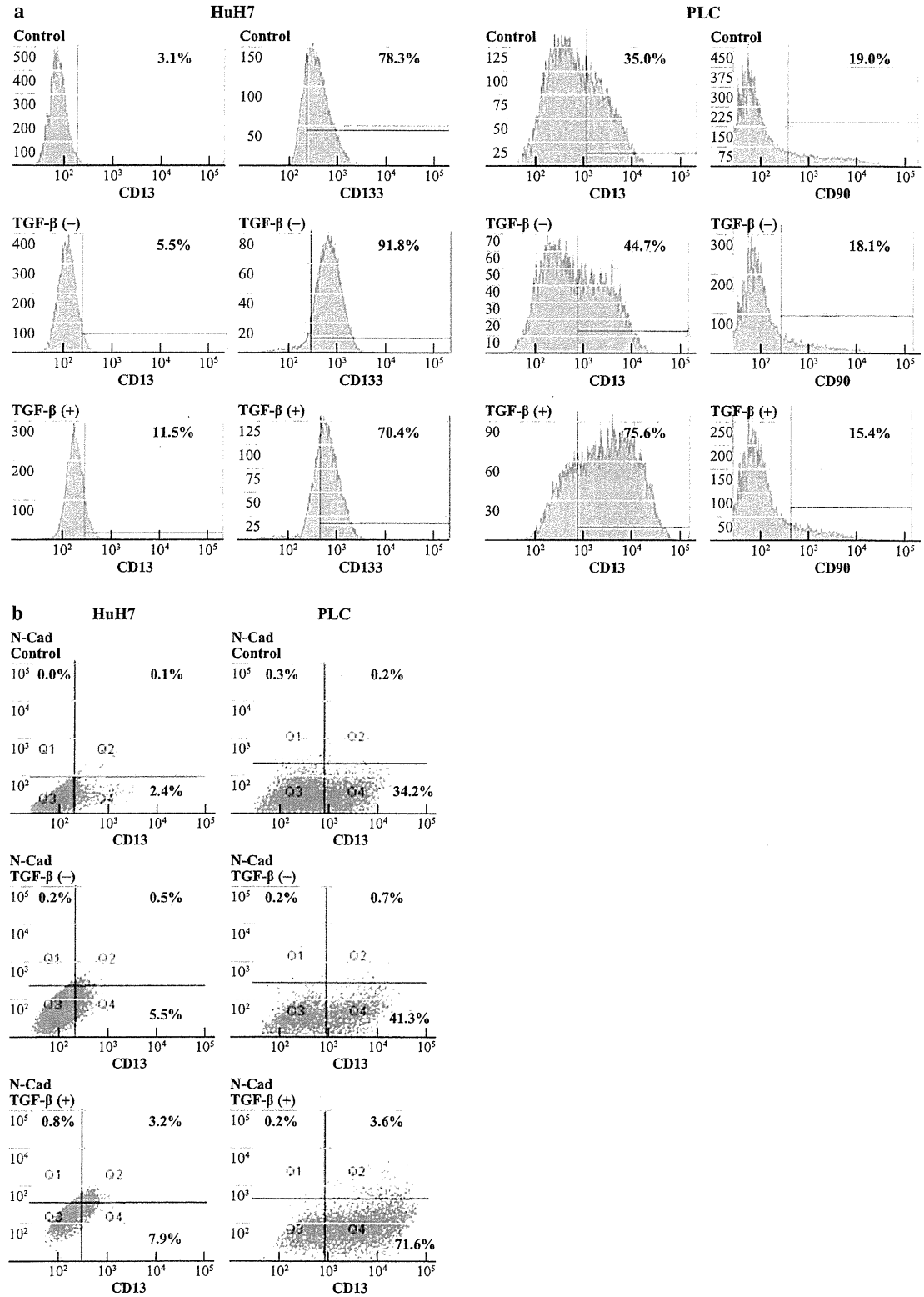

FIG. 2 TGF-β-induced EMT is associated with increased CD13 expression. **a** Expression of CD13 and CD133 in HuH7 cells (*upper*), and CD13 and CD90 in PLC cells (*lower*). *Each number* shows percentage of positive fraction of each marker. HuH7 cells: treated with 1 ng/ml of TGF-β. PLC cells: treated with 2 ng/ml of TGF-β. Control: cells were cultured in conditional medium containing with 10% FBS. **b** Expression analysis of N-cadherin (N-cad) and CD13 with or without TGF-β treatment

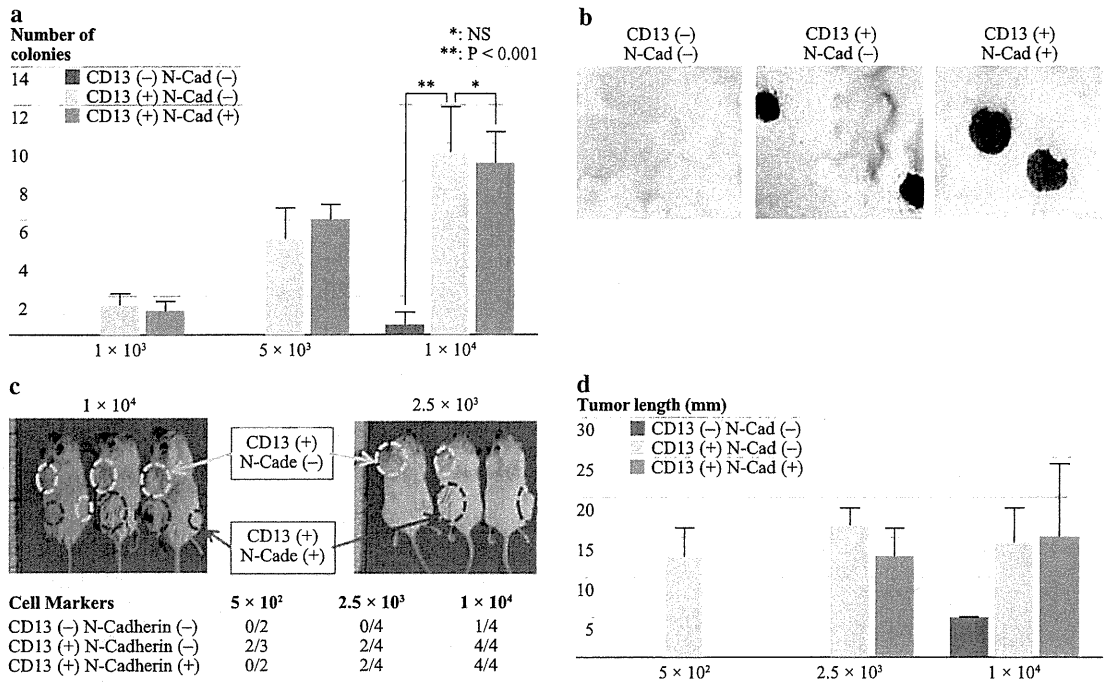

Cell Markers	5 × 10²	2.5 × 10³	1 × 10⁴
CD13 (–) N-Cadherin (–)	0/2	0/4	1/4
CD13 (+) N-Cadherin (–)	2/3	2/4	4/4
CD13 (+) N-Cadherin (+)	0/2	2/4	4/4

FIG. 3 $CD13^+$ liver cancer cells have higher tumorigenicity than $CD13^-$ cells. **a** Soft agar colony formation assay. After stimulation by TGF-β in culture, cells were isolated by FACS and indicated numbers of cells were subjected to assay. **b** Formed colonies (*bar*, 500 μm). **c** Limiting dilution assay. The indicated numbers of CD13 + PLC liver cancer cells were inoculated into NOD/SCID mice. **d** The resultant tumor volumes

CSCs and liver CSCs have been reported.[21,33] To study the change of ROS status during EMT, intracellular ROS levels were measured by pro-oxidants using the 2′,7′-dichlorofluorescein diacetate (DCF-DA) stain. The data indicated that ROS level in $CD13^+$ cells was low compared with that in $CD13^-$ cells. ROS level of $CD13^+$/N-cadherin$^+$ cells was higher than that of $CD13^+$/N-cadherin$^-$ cells, suggesting that the TGF-β–induced EMT process is associated with an increase of ROS level (Fig. 4a). With regard to ROS scavengers in these cells, the qRT-PCR data indicated that the expression of *GCLM* and *GSS* was high in the $CD13^+$/N-cadherin$^-$ cells compared with the $CD13^-$/N-cadherin$^-$ cells (Fig. 4b). Interestingly, expression of *GCLM* and *GSS* was low in $CD13^+$/N-cadherin$^+$ cells compared with $CD13^+$/N-cadherin$^-$ cells (Fig. 4b), suggesting that TGF-β/EMT-induced ROS were metabolized to the appropriate level mainly via the CD13 function, rather than via the actions of the other scavengers, *GCLM* and *GSS*.

We speculated that the survival of TGF-β–induced EMT cells might be dependent on CD13 function. To confirm the involvement of ROS in TGF-β-induced EMT cells, cells were treated with the antioxidant *N*-acetylcysteine (NAC) in culture and measured resulting ROS level. By TGF-β treatment, expression of the N-cadherin, fibronectin, and vimentin was increased, but with NAC treatment, expression of N-cadherin and fibronectin was reduced (Fig. 4c). In contrast, expression of vimentin was increased by NAC with TGF-β treatment, suggesting that increased levels of ROS induce EMT, but should be controlled at suitable levels to sufficient induction of ROS.

To assess the effect of CD13 inhibition on TGF-β-induced EMT, cells were cultured in a medium containing ubenimex, which is an inhibitor of CD13. The data indicated that inhibition of CD13 by ubenimex elicited cell death and consequently suppressed N-cadherin in a dose-dependent manner (Fig. 4d). Additionally, as $CD13^+$ cells were enriched by TGF-β treatment, they were reduced by TGF-β with NAC treatment (Fig. 4e). We concluded that CD13 plays a role in the TGF-β-induced EMT properties of CD13 + liver cancer cells analyzed in the present study.

TGF-β-Induced $CD13^+$ Cells with Stem Cell Properties

We studied the expression of the stemness genes B lymphoma Mo-MLV insertion region 1 homolog (*BMI1*) and translocation-associated notch protein TAN-1 (*NOTCH1*). The data indicated that *BMI1* expression was significantly higher in $CD13^+$/N-cadherin$^+$ cells than in

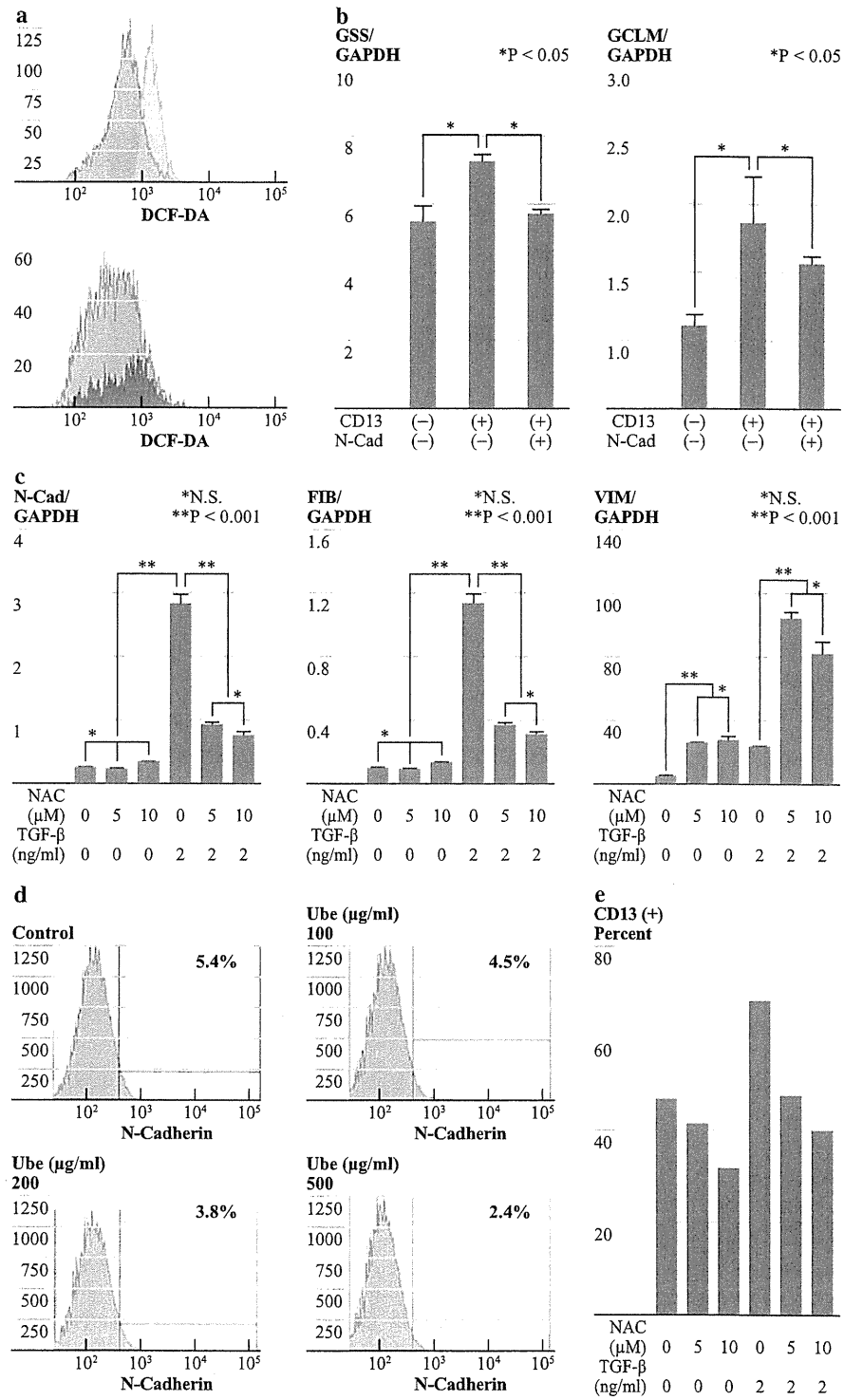

FIG. 4 TGF-β increase intracellular ROS level and induce EMT. **a** ROS level was measured after TGF-β exposure in culture. ROS level was detected by DCF-DA in the $CD13^+$, $CD13^-$, $CD13^+$N-cadherin$^-$, and $CD13^+$N-cadherin$^+$ fractions, as indicated. **b** qRT-PCR analysis of GSS and GCLM in $CD13^+$N-cadherin$^-$, $CD13^+$N-cadherin$^-$, and $CD13^+$N-cadherin$^+$ fractions. **c** Expression analysis of N-cadherin (N-cad), fibronectin (FIB), and vimentin (VIM) by qRT-PCR. Cells were treated by NAC with or without TGF-β in culture as indicated concentration. **d** Cells were cultured in medium containing ubenimex, an inhibitor of CD13, as indicated concentration and expression of N-cadherin was assessed. *Each number* indicates the percentage of N-cadherin expressing cells in each condition. **e** Expression of CD13 after treatment of NAC with or without TGF-β in culture as indicated concentration

$CD13^-$/N-cadherin$^-$ cells. Similarly, *NOTCH1* expression was significantly higher in $CD13^+$/N-cadherin$^+$ cells than in $CD13^+$/N-cadherin$^-$ cells, although expression in $CD13^+$/N-cadherin$^-$ cells was still significantly higher than that in $CD13^-$/N-cadherin$^-$ cells (Fig. 5a). Taken together that $CD13^+$/N-cadherin$^+$ cells have high tumorigenic ability next to $CD13^+$/N-cadherin$^-$ cells but express highest *BMI1* and *NOTCH1* expression, it can be thought that CD13+/N-cadherin + cells acquired stemness activity during EMT process induced by TGF-β.

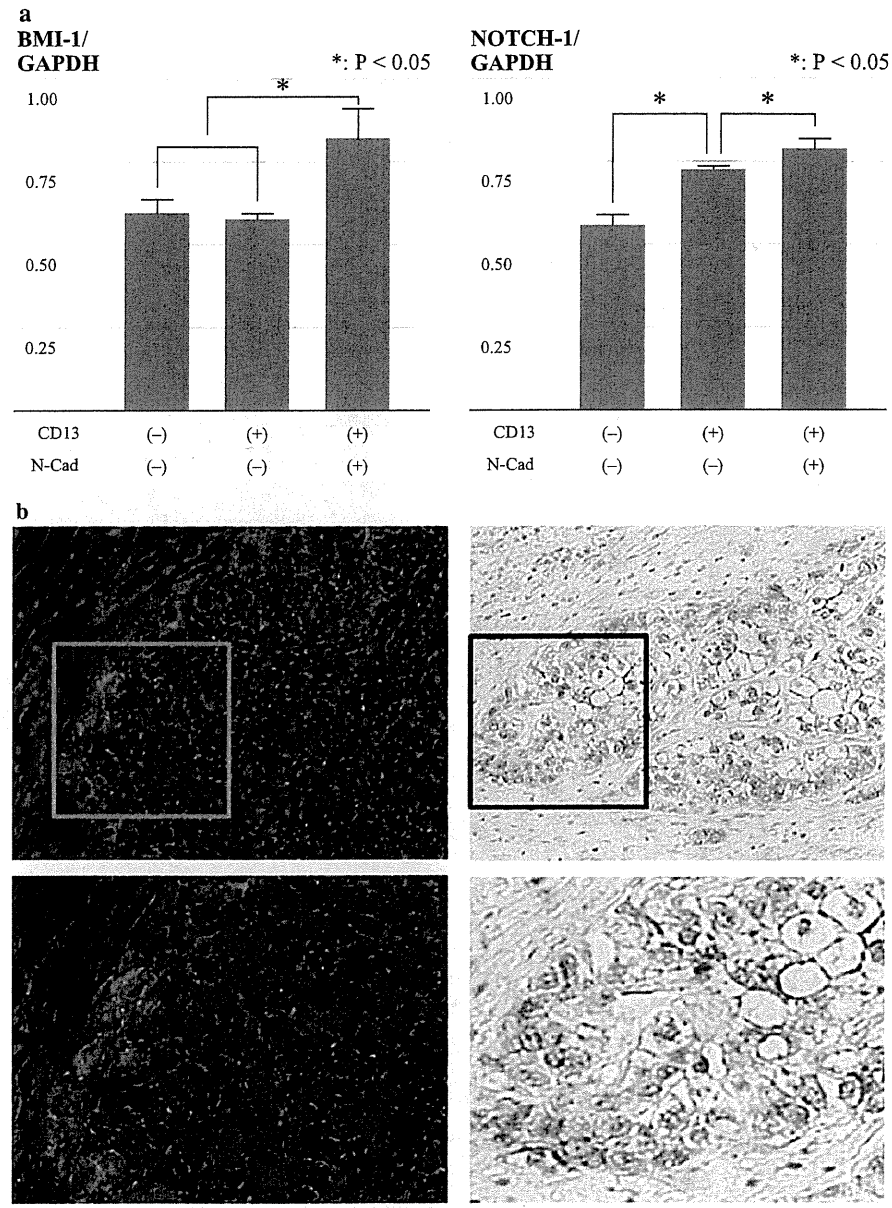

FIG. 5 CD13 and N-cadherin expression in human HCC sample. **a** Expression of BMI-1 and NOTCH1 in $CD13^{+}$N-$cadherin^{-}$, $CD13^{+}$N-$cadherin^{-}$, and $CD13^{+}$N-$cadherin^{+}$ fractions. After stimulation by TGF-β in culture, cells were isolated by FACS, RNA was extracted and qRT-PCR was performed. **b** Immunohistochemical analysis of post-TACE HCC sample stained with anti-human CD13 (*red*) and DAPI (*blue*) for the nucleus (*left*) and N-cadherin (*right*). *Lower panel* shows a higher magnification (×40) of the *square* in *upper column* (×10)

$CD13^{+}$/N-$cadherin^{+}$ Cells are Expressed in Therapy-Resistant HCC Cells

In the previous study, we have reported that CD13 + cells form cellular cluster along to fibrous capsule, especially after post-transcatheter arterial lipiodol chemoembolization (TACE) therapy.[21] To study N-cadherin expression in clinical hepatocellular carcinoma (HCC) sample, ten samples of HCC resected after TACE were used following study (Supplemental Table 1). Because CD13 was hard to detect in formalin-fixed sample, frozen sample was used to detect CD13 + cells. Our data indicated that, in all of the post-TACE samples examined, CD13 was found on the cell surface and N-cadherin expression was high (representative data shown in Fig. 5b). The surviving areas within the fibrous capsule of HCC tissue specimens taken after chemotherapy contained regions positive for both CD13 and N-cadherin; CD13 was expressed in adjacent regions of the HCC cells and formed bile canaliculi. Analysis of serial sections indicated that CD13 expression was combined with membrane expression of N-cadherin. The present data indicate that highly tumorigenic $CD13^{+}$/N-$cadherin^{+}$ HCC cells survive within the fibrous capsule of HCC tissues, suggesting that they are involved in therapy resistance and the aggressive behaviors of tumor cells after TACE.

DISCUSSION

Numerous reports have indicated that CSCs play a critical role in the generation of chemoradiation resistance.[1,2] Hence the findings that the EMT process could induce stemness in $CD24^+/CD44$ (low) CSC fractions in breast cancer, in $CD24^+/CD44^+/CD133^+$/Aldehyde Dehydrogenase$^+$ CSCs in pancreatic adenocarcinomas, and in $CD44^+/CD24^-$ CSCs in prostate cancer indicate a new epoch in cancer therapy.[27,34,35] Although our understanding of the link between therapy resistance, EMT, and metastasis remains unclear, in the present study, we show for the first time the functional relevance of CSC markers in the EMT phenomenon; our data suggest that in liver cancer, the functional CSC marker CD13 plays a role in the reduction of intracellular ROS, which has been shown to contribute to drug resistance.[21]

Emerging evidence supports the notion that EMT is an important step in tumor invasion and metastasis and is intimately involved in de novo and acquired chemoradiation resistance.[36] Consistent with this, the present data indicated that TGF-β exposure could induce the EMT phenotype but also elicit an increase in intracellular ROS and that this was reverted by the addition of a strong antioxidant (NAC) in culture. Recently, ROS have been found to be associated with tumor metastasis via tumor cell migration, invasion, and angiogenesis.[36] Thus, our findings suggest that strong chemopreventive agents antagonizing ROS could be useful for targeted reversal of EMT, which could become a novel approach for the prevention of tumor progression and metastasis. However, this type of inhibition would not kill CSCs but just suppress the cells. We also noted that an acute blockade of CD13, a natural, mild scavenger of intracellular ROS, in CD13-dependent malignant CSCs resulted in the induction of apoptosis,[21] suggesting the possible elimination of deleterious clones. The data suggest that a situation could arise wherein CSCs become accustomed to a relatively high level of intracellular ROS and are dependent on CD13 expression for the regulation of ROS levels; they survive by avoiding apoptosis. Thus, combining conventional chemotherapies, such as proliferation antagonizing 5-FU, with CSC-targeted reagents, such as ubenimex, may be beneficial for efficient tumor elimination.

Although simultaneous administration of 5-FU and ubenimex has been reported to have a synergic effect on tumor growth, the biological function of CD13 in liver CSCs remains to be elucidated.[21] To study the effect of CD13 inhibition on TGF-β-induced EMT, we cultured cells in a medium containing ubenimex, an inhibitor of CD13. Our data indicate that inhibition of CD13 by ubenimex elicited cell death and consequently resulted in dose-dependent suppression of N-cadherin, suggesting that CD13 plays a role in TGF-β-induced EMT properties in the $CD13^+$ liver cancer cells.

As biosynthesis, our data indicate that TGF-β stimulation elicits N-cadherin expression (EMT) as well as CD13 expression, presumably via the involvement of glycolysis and oxidative stress-responsive transcription factor c-Maf upstream of the CD13 gene's promoter (MAF-recognition element, MARE; Supplemental Fig. 1a and b), indicating that in the microenvironment of heterogeneous tumors, hypoxic conditions could increase the secretion of cytokines, such as IL6 and TGF-β from mesenchymal cells.[37,38] In cancer cells, these stimulate the response of Stat3 and hypoxia-inducible factors (HIFs) downstream of IL6 and of Smad4 downstream of TGF-β.[38] These in turn are involved in the transcriptional regulation of the proto-oncogene *c-MAF*, presumably via p300/CEBPbeta, AP1, and nuclear factor (NF) kappa B sites in its gene promoter.[38–41] Consequently, the present study proposes a natural working hypothesis where the hypoxic and inflammatory conditions in the microenvironment elicit cellular responses to increased CD13 expression that are beneficial for the survival of EMT-stimulated CSCs.

Although the majority of the experiments in this study are based on cell lines, the expression and ROS analyses support the contention that PLC cells reflect clinical HCC and may hold promise for preclinical studies. This study also suggests that the future development of liver cancer therapy based on CSC and EMT concepts appears promising. We are undertaking further analyses of clinical HCC samples to provide the necessary confirmation of our contention using in vivo assays.

ACKNOWLEDGMENT This study was supported in part by a grant from Core Research for Evolutional Science and Technology (CREST), a Grant-in-Aid for scientific research on Priority Areas (20012039), Grants-in-Aid for scientific research S (21229015) and C (20590313) from the Ministry of Education, Culture, Sports, Science, and Technology, and a grant from the Tokyo Biochemical Research Foundation, Japan.

REFERENCES

1. Sagar J, Chaib B, Sales K, Winslet M, Seifalian A. Role of stem cells in cancer therapy and cancer stem cells: a review. *Cancer Cell Int.* 2007;4:7–9.
2. Reya T, Morrison SJ, Clarke MF, Weissman IL. Stem cells, cancer, and cancer stem cells. *Nature.* 2001;414(6859):105–11.
3. Tan BT, Park CY, Ailles LE, Weissman IL. The cancer stem cell hypothesis: a work in progress. *Lab Invest.* 2006;86(12):1203–7.
4. Wulf GG, Wang RY, Kuehnle I, et al. A leukemic stem cell with intrinsic drug efflux capacity in acute myeloid leukemia. *Blood.* 2001;98(4):1166–73.
5. Lapidot T, Sirard C, Vormoor J, et al. A cell initiating human acute myeloid leukaemia after transplantation into SCID mice. *Nature.* 1994;367(6464):645–8.

6. Bonnet D, Dick JE. Human acute leukemia is organized as a hierarchy that originates from a primitive hematopoietic cell. *Nat Med.* 1997;3(7):730–7.
7. Piccirillo SG, Reynolds BA, Zanetti N, et al. Bone morphogenetic proteins inhibit the tumorigenic potential of human brain tumour-initiating cells. *Nature.* 2006;444(7120):761–5.
8. Bao S, Wu Q, McLendon RE, et al. Glioma stem cells promote radioresistance by preferential activation of the DNA damage response. *Nature.* 2006;444(7120):756–60.
9. Prince ME, Sivanandan R, Kaczorowski A, et al. Identification of a subpopulation of cells with cancer stem cell properties in head and neck squamous cell carcinoma. *Proc Natl Acad Sci USA.* 2007;104(3):973–8.
10. Al-Hajj M, Wicha MS, Benito-Hernandez A, Morrison SJ, Clarke MF. Prospective identification of tumorigenic breast cancer cells. *Proc Natl Acad Sci USA.* 2003;100(7):3983–8.
11. Ricci-Vitiani L, Lombardi DG, Pilozzi E, et al. Identification and expansion of human colon-cancer-initiating cells. *Nature.* 2007;445(7123):111–5.
12. O'Brien CA, Pollett A, Gallinger S, Dick JE. A human colon cancer cell capable of initiating tumour growth in immunodeficient mice. *Nature.* 2007;445(7123):106–10.
13. Haraguchi N, Utsunomiya T, Inoue H, et al. Characterization of a side population of cancer cells from human gastrointestinal system. *Stem Cells.* 2006;24(3):506–13.
14. Chiba T, Kita K, Zheng YW, et al. Side population purified from hepatocellular carcinoma cells harbors cancer stem cell-like properties. *Hepatology.* 2006;44(1):240–51.
15. Ding W, Mouzaki M, You H, et al. CD133 + liver cancer stem cells from methionine adenosyl transferase 1A-deficient mice demonstrate resistance to transforming growth factor (TGF)-beta-induced apoptosis. *Hepatology.* 2009;49(4):1277–86.
16. Ma S, Chan KW, Hu L, et al. Identification and characterization of tumorigenic liver cancer stem/progenitor cells. *Gastroenterology.* 2007;132(7):2542–56.
17. Zhu Z, Hao X, Yan M, et al. Cancer stem/progenitor cells are highly enriched in CD133(+)CD44(+) population in hepatocellular carcinoma. *Int J Cancer.* 2010;126(9):2067–78.
18. Yang ZF, Ngai P, Ho DW, et al. Identification of local and circulating cancer stem cells in human liver cancer. *Hepatology.* 2008;47(3):919–28.
19. Yang ZF, Ho DW, Ng MN, et al. Significance of CD90 + cancer stem cells in human liver cancer. *Cancer Cell.* 2008;13(2):153–66.
20. Yamashita T, Ji J, Budhu A, et al. EpCAM-positive hepatocellular carcinoma cells are tumor-initiating cells with stem/progenitor cell features. *Gastroenterology.* 2009;136(3):1012–24.
21. Haraguchi N, Ishii H, Mimori K, et al. CD13 is a therapeutic target in human liver cancer stem cells. *J Clin Invest.* 2010;120(9):3326–39.
22. Menrad A, Speicher D, Wacker J, Herlyn M. Biochemical and functional characterization of aminopeptidase N expressed by human melanoma cells. *Cancer Res.* 1993;53(6):1450–5.
23. Pasqualini R, Koivunen E, Kain R, et al. Aminopeptidase N is a receptor for tumor-homing peptides and a target for inhibiting angiogenesis. *Cancer Res.* 2000;60(3):722–7.
24. Mishima Y, Matsumoto-Mishima Y, Terui Y, et al. Leukemic cell-surface CD13/aminopeptidase N and resistance to apoptosis mediated by endothelial cells. *J Natl Cancer Inst.* 2002;94(13):1020–8.
25. Thiery JP, Acloque H, Huang RY, Nieto MA. Epithelial-mesenchymal transitions in development and disease. *Cell.* 2009;139(5):871–90.
26. Yang J, Weinberg RA. Epithelial-mesenchymal transition: at the crossroads of development and tumor metastasis. *Dev Cell.* 2008;14(6):818–29.
27. Mani SA, Guo W, Liao MJ, et al. The epithelial-mesenchymal transition generates cells with properties of stem cells. *Cell.* 2008;133(4):704–15.
28. Wu WS. The signaling mechanism of ROS in tumor progression. *Cancer Metastasis Rev.* 2006;25(4):695–705.
29. Radisky DC, Levy DD, Littlepage LE, et al. Rac1b and reactive oxygen species mediate MMP-3-induced EMT and genomic instability. *Nature.* 2005;436(7047):123–7.
30. Rees JR, Onwuegbusi BA, Save VE, Alderson D, Fitzgerald RC. In vivo and in vitro evidence for transforming growth factor-beta1-mediated epithelial to mesenchymal transition in esophageal adenocarcinoma. *Cancer Res.* 2006;66(19):9583–90.
31. Ito K, Hirao A, Arai F, et al. Regulation of oxidative stress by ATM is required for self-renewal of haematopoietic stem cells. *Nature.* 2004;431(7011):997–1002.
32. Ito K, Hirao A, Arai F, et al. Reactive oxygen species act through p38 MAPK to limit the lifespan of hematopoietic stem cells. *Nat Med.* 2006;12(4):446–51.
33. Diehn M, Cho RW, Lobo NA, et al. Association of reactive oxygen species levels and radioresistance in cancer stem cells. *Nature.* 2009;458(7239):780–3.
34. Dembinski JL, Krauss S. Characterization and functional analysis of a slow cycling stem cell-like subpopulation in pancreas adenocarcinoma. *Clin Exp Metastasis.* 2009;26(7):611–23.
35. Klarmann GJ, Hurt EM, Mathews LA, et al. Invasive prostate cancer cells are tumor initiating cells that have a stem cell-like genomic signature. *Clin Exp Metastasis.* 2009;26(5):433–46.
36. Wang Z, Li Y, Sarkar FH. Signaling mechanism(s) of reactive oxygen species in epithelial–mesenchymal transition reminiscent of cancer stem cells in tumor progression. *Curr Stem Cell Res Ther.* 2010;5(1):74–80.
37. Mahoney KM, Petrovic N, Schacke W, Shapiro LH. CD13/APN transcription is regulated by the proto-oncogene c-Maf via an atypical response element. *Gene.* 2007;403(1–2):178–87.
38. Nilsson CL, Dillon R, Devakumar A, et al. Quantitative phosphoproteomic analysis of the STAT3/IL-6/HIF1alpha signaling network: an initial study in GSC11 glioblastoma stem cells. *J Proteome Res.* 2010;9(1):430–43.
39. Kataoka K. Multiple mechanisms and functions of Maf transcription factors in the regulation of tissue-specific genes. *J Biochem.* 2007;141(6):775–81.
40. Cvekl A, Yang Y, Chauhan BK, Cveklova K. Regulation of gene expression by Pax6 in ocular cells: a case of tissue-preferred expression of crystalines in lens. *Int J Dev Biol.* 2004;48(8–9):829–44.
41. Hiramatsu Y, Suto A, Kashiwakuma D, et al. c-Maf activates the promoter and enhancer of the IL-21 gene, and TGF-b inhibits c-Maf-induced IL-21 production in CD4+T cells. *J Leukoc Biol.* 2010;87(4):703–12.

Ann Surg Oncol
DOI 10.1245/s10434-011-1739-7

Annals of
SURGICAL ONCOLOGY
OFFICIAL JOURNAL OF THE SOCIETY OF SURGICAL ONCOLOGY

ORIGINAL ARTICLE – TRANSLATIONAL RESEARCH AND BIOMARKERS

Absence of CD71 Transferrin Receptor Characterizes Human Gastric Adenosquamous Carcinoma Stem Cells

Masahisa Ohkuma, MD[1,2], Naotsugu Haraguchi, MD, PhD[1], Hideshi Ishii, MD, PhD[1,3], Koshi Mimori, MD, PhD[3], Fumiaki Tanaka, MD, PhD[3], Ho Min Kim, MD[1], Miho Shimomura, MD[1], Hajime Hirose, MD[1], Katsuhiko Yanaga, MD, PhD[2], and Masaki Mori, MD, PhD[1]

[1]Department of Gastroenterological Surgery, Graduate School of Medicine, Osaka University, Osaka, Japan; [2]Department of Surgery, Jikei University School of Medicine, Tokyo, Japan; [3]Department of Surgery, Medical Institute of Bioregulation, Kyushu University, Oita, Japan

ABSTRACT

Background. Although the importance of cancer stem cells (CSCs) in overcoming resistance to therapy and metastasis has recently been reported, the role of CSCs in gastric cancer remains to be elucidated.

Methods. MKN-1 cells were used to study markers of CSCs in gastric adenosquamous carcinoma, as these cells are suitable for determining multidifferentiation ability. Changes in expression of CD44, CD49f, CD133, and CD71 following 5-fluorouracil (5-FU) treatment were assessed.

Results. After 5-FU treatment, only the $CD71^-$ fraction was significantly increased. Investigation of CD71 indicated that the $CD71^-$ cell fraction was present in the G1/G0 cell cycle phase and showed high resistance to the anticancer agent 5-FU. Limiting dilution and serial transplantation assays revealed the $CD71^-$ cell fraction to have higher tumorigenicity than the $CD71^+$ cell fraction. The $CD71^-$ cell fraction showed multipotency to adenocarcinoma and squamous cell carcinoma. A three-dimensional (3D) invasion assay and immunohistochemical analysis showed $CD71^-$ cells to be highly invasive and to exist in the invasive fronts of cancer foci.

Conclusion. The present study suggests that use of $CD71^-$ as a marker for adenosquamous carcinoma may provide a useful model for studying CSCs.

First Received: 9 September 2010

H. Ishii, MD, PhD
e-mail: hishii@gesurg.med.osaka-u.ac.jp

M. Mori, MD, PhD
e-mail: mmori@gesurg.med.osaka-u.ac.jp

Published online: 27 April 2011

Recent studies have identified a small fraction of cancer stem cells (CSCs) that are capable of self-renewal and multipotency and play a role in tumor progression.[1–4] Although "total cell kill therapy" reduces tumor size, the malignant cells that survive are believed to include CSCs, resulting in clinically important consequences such as metastasis, relapse, and resistance to therapy.[1–4] Gastric cancer is relatively common in East Asia and South America. It is the fourth most frequently diagnosed malignant tumor in the world and the second most lethal disease after lung cancer.[5] There are few implications for the markers of CSCs in gastric cancer except CD44 and side population (SP) cells.[6,7] To the best of our knowledge, to date no report has focused on the multipotency of gastric cancer CSCs. Although adenosquamous carcinoma is believed to represent less than 1% of all gastric cancers, it is a good model for understanding the mechanism underlying the multipotency of CSCs as well as cellular hierarchy.

MATERIALS AND METHODS

Cell Preparation and Culture

MKN-1 cells were obtained from the Japanese Collection of Research Bioresources Cell Bank. Cells were cultured in Roswell Park Memorial Institute (RPMI) 1640 medium (Invitrogen)/10% fetal bovine serum (FBS) containing 100 μg/ml penicillin G and 100 units/ml streptomycin at 37°C in 5% CO_2 atmosphere. Four samples of human gastric adenosquamous carcinoma were obtained from Kyushu University in Japan with the approval of the Research Ethics Board at the university and the informed consent of the patients. To obtain tumor cells from xenografted mice, tumors were digested with 2 mg/ml collagenase A (Roche Diagnostics) solution.

Flow Cytometry Analysis

After FcR blocking (Miltenyi Biotec), cells were stained with the following anti-human antibodies: phycoerythrin (PE)-CD71 (BD Biosciences), allophycocyanin (APC)-CD133/1 (Miltenyi Biotec), PE-CD44 (BD Pharmingen), and PE-CD49f (BD Pharmingen), and isotype control antibody (BD Biosciences). After doublet cell elimination, dead cells were eliminated using 7-amino actinomycin D. FACSVantage SE DiVa (Becton Dickinson) and FACS SORP Aria (Becton Dickinson) were used for analysis and cell sorting. To isolate human cells from mouse xenografts, biotinylated anti-mouse H-2Kd (BD Pharmingen) and biotinylated anti-mouse CD45 (BD Pharmingen) antibodies were used. Streptavidin-APC-Cy7 (BD Pharmingen) was used as the secondary antibody.

Cell Cycle Assay

To characterize SP fractions, 1×10^6 cells were labeled with 10 μg/ml Hoechst 33342 (Invitrogen) in a staining medium at 37°C for 70 min alone or with 50 μM Fumitremorgin C (Sigma-Aldrich). For cell cycle assays, cells were labeled with Hoechst 33342 (Invitrogen) at concentration of 5–10 μg/ml for 60–90 min at 37°C. Data were analyzed using Diva software (Becton Dickinson) and FlowJo software version 7.2 (Tree Star Inc.).

Colony Formation Assay

Cells were plated at density of 500–1,000 cells/well in three 35-mm plates (BD Falcon) and were stained on day 14 using the Diff-Quik kit (Sysmex Corp.).

Cell Proliferation Assay

Cell proliferation was examined on days 1, 3, 5, 7, and 9. Isolated cells were seeded into 96-well culture plates at 1×10^3 cells/well. After 72 h, cell viability was determined by an adenosine triphosphate (ATP) bioluminescence assay (CellTiter-Glo Luminescent Cell Viability Assay; Promega). Luminescence signals were detected using a luminometer (VICTOR3 Multilabel Plate Counter, PerkinElmer).

Migration and Invasion Assays

For migration and invasion assays, the cells (2.5×10^4 cells/well) were placed in the upper chamber of a BD BioCoat tumor invasion system (Becton Dickinson), and the lower chamber was filled with a culture medium containing 10% FBS. The membranes were labeled using calcein AM solution after 72 h of incubation.

3D Culturing

After sorting, the cells were plated on 24-well plates coated with Matrigel (BD Biosciences) at density of 5×10^3/ml and cultured for 21 days in a medium that was changed every 72 h.

Transplantation of Cancer Cells

The isolated cells were resuspended in 1:1 mixture of medium and Matrigel (BD Biosciences) to final volume of 200 μl. Tumor cells were injected into the bilateral axillary fossa of 4-week-old female nonobese diabetic/severe combined immunodeficiency (NOD/SCID) mice under anesthesia. Eight weeks after inoculation, the grafts were removed for further studies.

Immunohistochemistry

Paraffin-embedded tissue sections were stained with anti-human MUC6 (Thermo Scientific), anti-human CK5/6 (DakoCytomation), and anti-human CD71 (Thermo Scientific) antibodies. Antibodies were detected using Envision reagents (EnVision + Dual Link System-HRP; DakoCytomation).

Statistical Analysis

For continuous variables, data are expressed as mean ± standard deviation (SD). Differences between groups were estimated by Student's *t*-test and repeated-measures analysis of variance (ANOVA). All differences were deemed significant at a level of $P < 0.05$.

RESULTS

Assessment of CSC Markers Using Anticancer Drugs

Previous reports have indicated that CSCs are resistant to chemotherapy.[1–4] Repeated exposure to anticancer drugs is believed to enhance the survival of CSCs while other daughter cells are inhibited, which leads to accumulation of the CSC fraction. Therefore, we assessed the response of MKN-1 cells on exposure to the anticancer drug 5-fluorouracil (5-FU) that is generally used in treating tumors of the digestive system.[8,9] After culturing MKN-1 cells in a growth medium with or without 5 μg/ml 5-FU for 7 days, changes in expression of cell surface markers were assessed. We evaluated CD44, CD49f, CD133, and CD71 as candidate markers; these have been reported as CSC markers for other organs or normal stem cells.[10–15] Following treatment with 5-FU, expressions of CD44, CD49f,

and CD133 were unaltered compared with those of the controls. On the other hand, the $CD71^-$ fraction increased from 18.6 to 82.0% after 5-FU treatment (Fig. 1). We then focused on the expression of CD71, because the $CD71^-$ fraction was enriched after 5-FU treatment.

Characterization of $CD71^-$ Cells In Vitro

As CSCs are typically characterized as capable of self-renewal, we studied their colony-forming capacity, which is assumed to reflect some aspects of self-reproduction.[1–4] The $CD71^-$ fraction showed profoundly higher colony-forming activity in vitro compared with that of the $CD71^+$ fraction (3.64-fold; $P < 0.05$; Fig. 2a).

Hematopoietic and leukemic stem cells exist in the G0/G1 cell cycle phase;[16–18] therefore, we examined the cell cycle status. Our data indicated that $CD71^-$ cells existed mainly in the G0/G1 phase (87.2 ± 2.53%), while $CD71^+$ cells existed mainly in the G2/M cell cycle phase (70.3 ± 5.61%; Fig. 2b).

To assess whether the $CD71^-$ cell population produced $CD71^+$ cells during cell proliferation, an isolated $CD71^-$ cell population was cultured to trace expression of CD71. The isolated $CD71^-$ cells rapidly produced $CD71^+$ cells within 1 week. The proportion of the $CD71^+$ cell fraction reached 80% in 10 days; the same percentage of the $CD71^+$ cell fraction was observed in the control MKN-1 cells. Conversely, the isolated and cultured $CD71^+$ cells produced a $CD71^-$ cell fraction of approximately 20% within 4 days of isolation. The proportion decreased to about 10% after 4 days (Fig. 2c). This was lower than the percentage of $CD71^-$ cells in the controls. $CD71^+$ and $CD71^-$ cells accounted for 81.4 and 18.6%, respectively, of control cells, suggesting that $CD71^+$ cells are less capable of producing $CD71^-$ cells.

Next, we assessed the scatter and invasive activities of sorted $CD71^+$ and $CD71^-$ cells. The scatter and invasive activities of $CD71^-$ cells were higher by 4.5- and 2.3-fold, respectively, than those of $CD71^+$ cells (Fig. 2d). To confirm the high cell migratory ability of $CD71^-$ cells, isolated $CD71^+$ and $CD71^-$ cells were seeded in a Matrigel-coated chamber and cultured for 21 days. Interestingly, $CD71^-$ cells formed spheroid-shaped and globular colonies, whereas $CD71^+$ cells formed small numbers of spheroid-shaped colonies, suggesting that $CD71^-$ cells possess high migratory and invasive potential (Fig. 2e).

As our data indicated that the $CD71^-$ population was resistant to 5-FU exposure, we considered the possibility that the drug exclusion activity of $CD71^-$ cells may be higher than that of $CD71^+$ cells. In the MKN-1 cell population, the percentage of the SP fraction was 5.8% (Fig. 2f), and 32.1% of the cells were $CD71^-$.

Tumorigenicity of $CD71^-$ Cells

To assess the tumorigenicity of $CD71^-$ and $CD71^+$ cells, isolated $CD71^+$ and $CD71^-$ cells were inoculated subcutaneously into NOD/SCID mice. Mice inoculated with 10,000, 5,000, and 2,500 $CD71^+$ or $CD71^-$ cells showed tumor formation after 8 weeks. Tumor initiation was more apparent among mice inoculated with 1,000 or 100 $CD71^-$ cells compared with mice inoculated with $CD71^+$ cells. In particular, when 100 cells were inoculated, all mice inoculated with the $CD71^-$ fraction developed

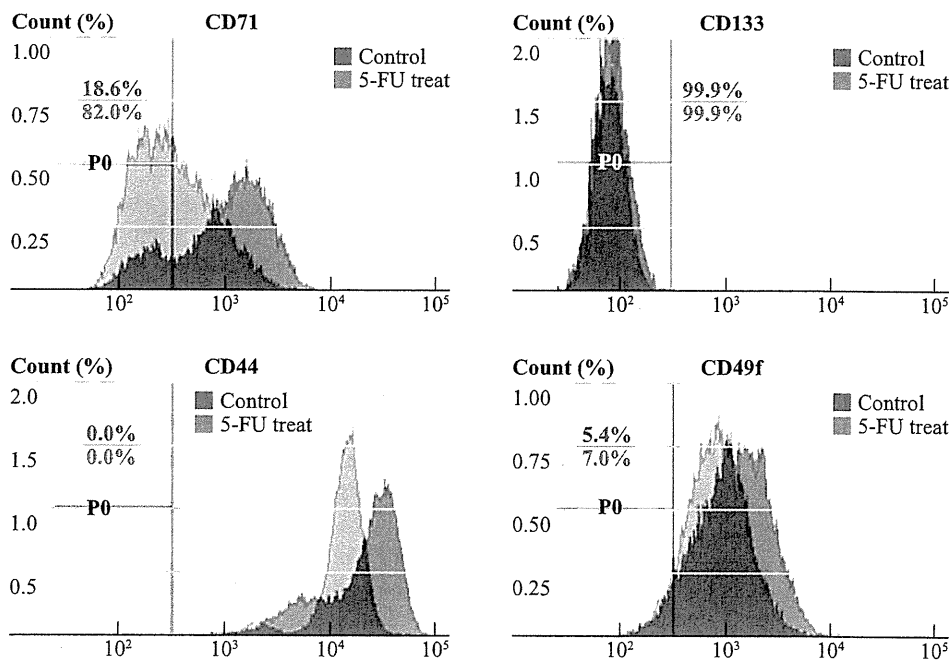

FIG. 1 $CD71^-$ cell fraction resistant to 5-FU treatment: Each panel displays the change in the CD71, CD133, CD44, and CD49f cell fractions after 5-FU treatment compared with controls. *Numbers* in each panel show the percentage of each negative cell fraction

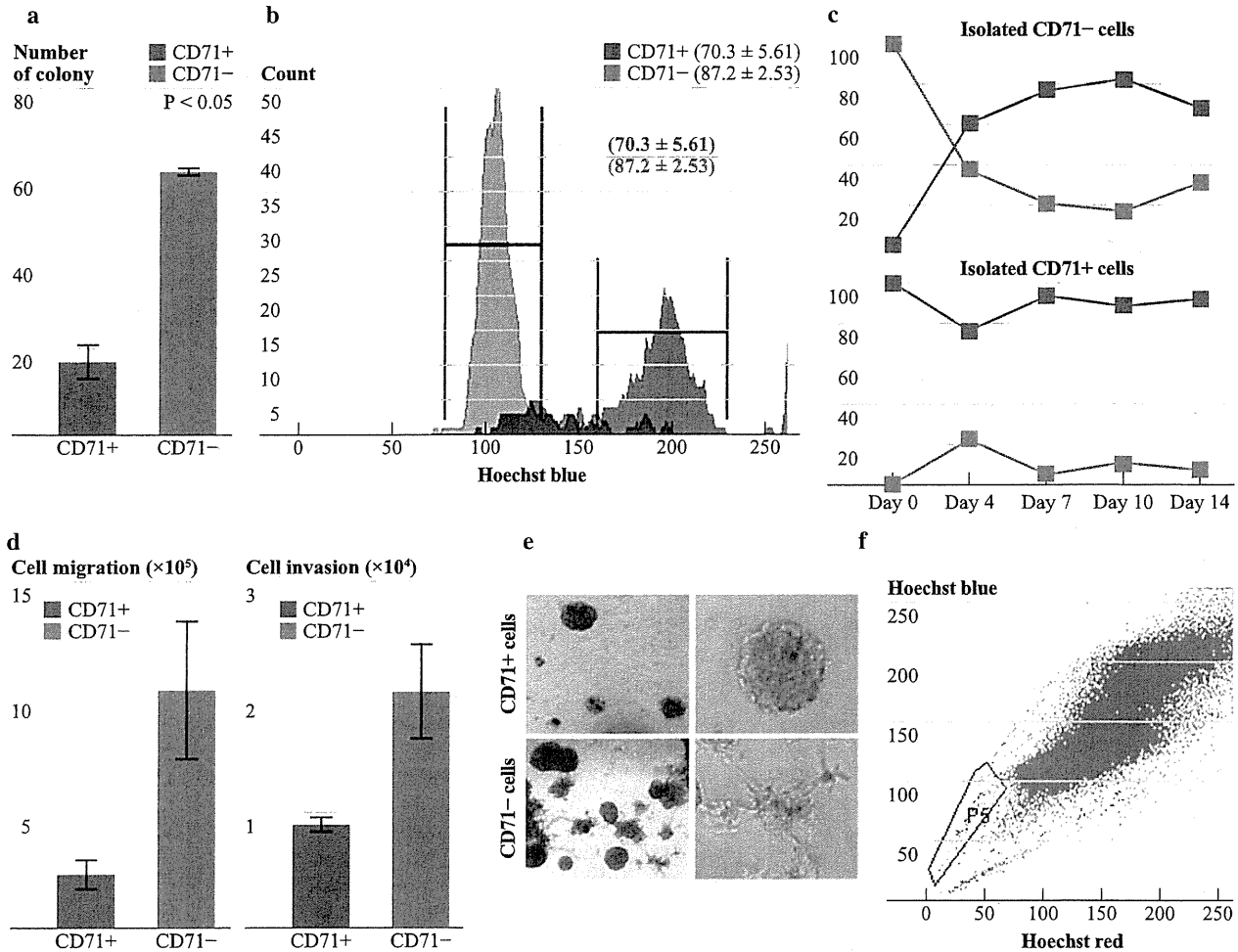

FIG. 2 CD71$^-$ cell fraction exists mainly in the G0/G1 cell cycle phase and shows high invasive ability: **a** Colony formation assay of isolated CD71$^-$ and CD71$^+$ cell fractions. Data are mean ± SD from independent experiments with differential fractions. $^*P < 0.05$. **b** Cell cycle assay of isolated CD71$^-$ and CD71$^+$ cell fractions. The number of the CD71$^-$ cell fraction (*red*) shows the percentage in G0/G1 cell cycle phase, and the number of the CD71$^+$ cell fraction (*blue*) shows the percentage in the G2/M cell cycle phase. **c** Time-course study of the changes in CD71 expression in isolated and cultured CD71$^-$ cells (*left*) and CD71$^+$ cells (*right*). **d** Cell migration (*left*) and invasive ability (*right*) of isolated CD71$^-$ and CD71$^+$ cell fractions. **e** 3D Matrigel culture of isolated CD71$^-$ and CD71$^+$ cell fractions. *Left column*, lower magnification (×10); *right column*, higher magnification (×20). *Bar* 100 μm. **f** Analysis of the SP fraction in MKN-1 cells

tumors (5/6, 83.3%), whereas none of the mice inoculated with the CD71$^+$ fraction developed tumors (0/6, 0%; Fig. 3a; Table 1). The size of the tumors formed was significantly larger in mice inoculated with 10,000, 1,000, and 100 CD71$^-$ cells than in mice inoculated with the CD71$^+$ fraction (Fig. 3b). Unfortunately, no metastatic lesions were observed in the CD71$^-$ and CD71$^+$ fraction-inoculated mice.

To assess tumorigenesis more definitively, a serial transplantation assay was performed. Similar to the results obtained with primary mice, the secondary mice developed tumors only after inoculation with 100 CD71$^-$ cells (3/5, 60%; Table 1; Fig. 3c). Tumorigenicity was relatively less than that in the primary mice, although the difference was apparent.

To assess whether CD71$^-$ cells produce CD71$^+$ cells in vivo, the tumors of CD71$^-$ cell-inoculated mice were digested to single cells and analyzed by flow cytometry. The data indicated that CD71$^-$ cell-derived tumors contained 21.6% CD71$^+$ cells, suggesting that CD71$^-$ cells produce CD71$^+$ cells (Fig. 3d). Interestingly, CD71$^+$ cell-derived tumors also contained CD71$^-$ cells (73.7%), suggesting that some part of the CD71$^+$ cell fraction produced CD71$^-$ cells (Fig. 3d).

Bipotentiality of CD71 Cells In Vivo

Histopathological examination revealed that tumor cells derived from isolated CD71$^-$ cells were heterogeneous with atypical nuclei and an apparently malignant

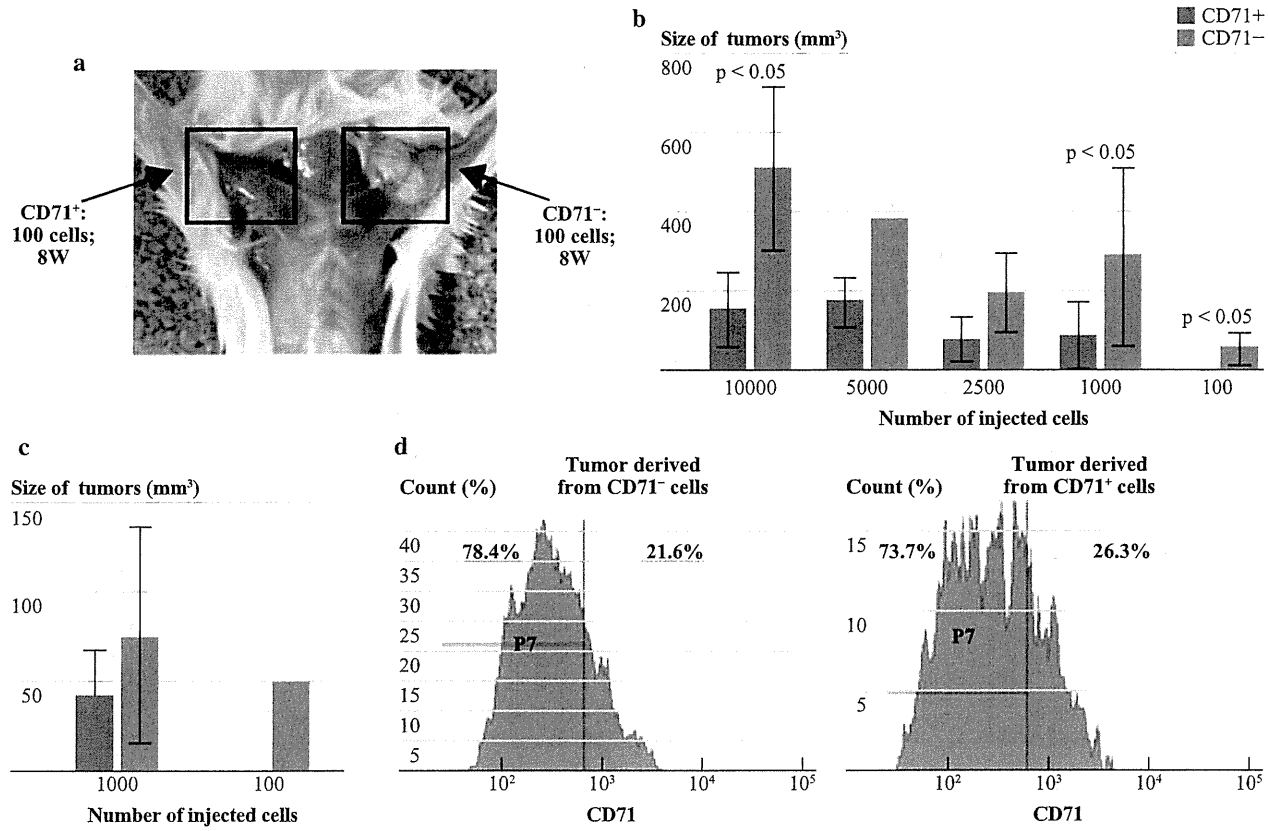

FIG. 3 $CD71^-$ cells have higher tumorigenicity: **a** Tumors formed from 100 isolated $CD71^-$ (*right solid square*) and $CD71^+$ (*left solid square*) fractions 8 weeks after inoculation into mice. **b** Tumor size derived from 10,000 to 100 isolated $CD71^-$ and $CD71^+$ cell fractions. Data are mean ± SD from independent experiments. $*P < 0.05$. **c** Tumor size and tumor formation of serially transplanted $CD71^-$ and $CD71^+$ cell fractions. **d** Flow cytometry analysis of CD71 expression of digested tumors derived from $CD71^-$ (*upper*) and $CD71^+$ (*lower*) cell fractions

TABLE 1 Limiting dilution and serial transplantation assays of the $CD71^-$ and $CD71^+$ cell fractions

	Cell fraction	Numbers of injected cells				
		100	1,000	2,500	5,000	10,000
Limiting dilution	$CD71^-$	5/6	10/10	3/3	2/2	4/4
	$CD71^+$	0/6	8/10	3/3	3/3	5/5
Serial transplantation	$CD71^-$	3/5	5/5	–	–	–
	$CD71^+$	0/5	3/5	–	–	–

phenotype, whereas tumor cells from $CD71^+$ cells were not (Fig. 4a).

We used immunohistochemical staining to assess whether $CD71^-$ cells showed multipotency. Staining with anti-MUC6, a differentiation marker for adenocarcinoma, showed that tumors derived from $CD71^-$ and $CD71^+$ cells were positive for MUC6. In contrast, staining with anti-CK 5/6, a differentiation marker for the squamous cell lineage, demonstrated that tumors from all three $CD71^-$ cell-inoculated mice (100%) were strongly positive for CK 5/6, whereas all the tumors (3/3, 100%) obtained from $CD71^+$ cell-inoculated mice were completely negative for CK 5/6 (Fig. 4b). These findings suggest that $CD71^-$ cells produced adenocarcinoma and squamous cell carcinoma, whereas $CD71^+$ cells contributed predominantly to adenocarcinoma. Pathologically, the tumors derived from the $CD71^-$ fraction were very similar to those derived from the parent cells.

To confirm CD71 expression in clinical adenosquamous gastric cancer cases, specimens were stained with CD71 antibody. In all four samples, expression of CD71 was typically recognized in the main cancer foci as a cell surface molecule (Fig. 4c). In the present study, $CD71^-$ cells showed higher migratory and invasive ability than $CD71^+$ cells (Fig. 2d, e). Invasive fronts suggest a critical role in the progression and metastasis of tumors. Interestingly, in the present study, immunohistochemical analysis of human gastric adenosquamous carcinoma demonstrated that $CD71^-$ cells were distributed in whole tumors as well as in cluster formations at invasive fronts (Fig. 4c).

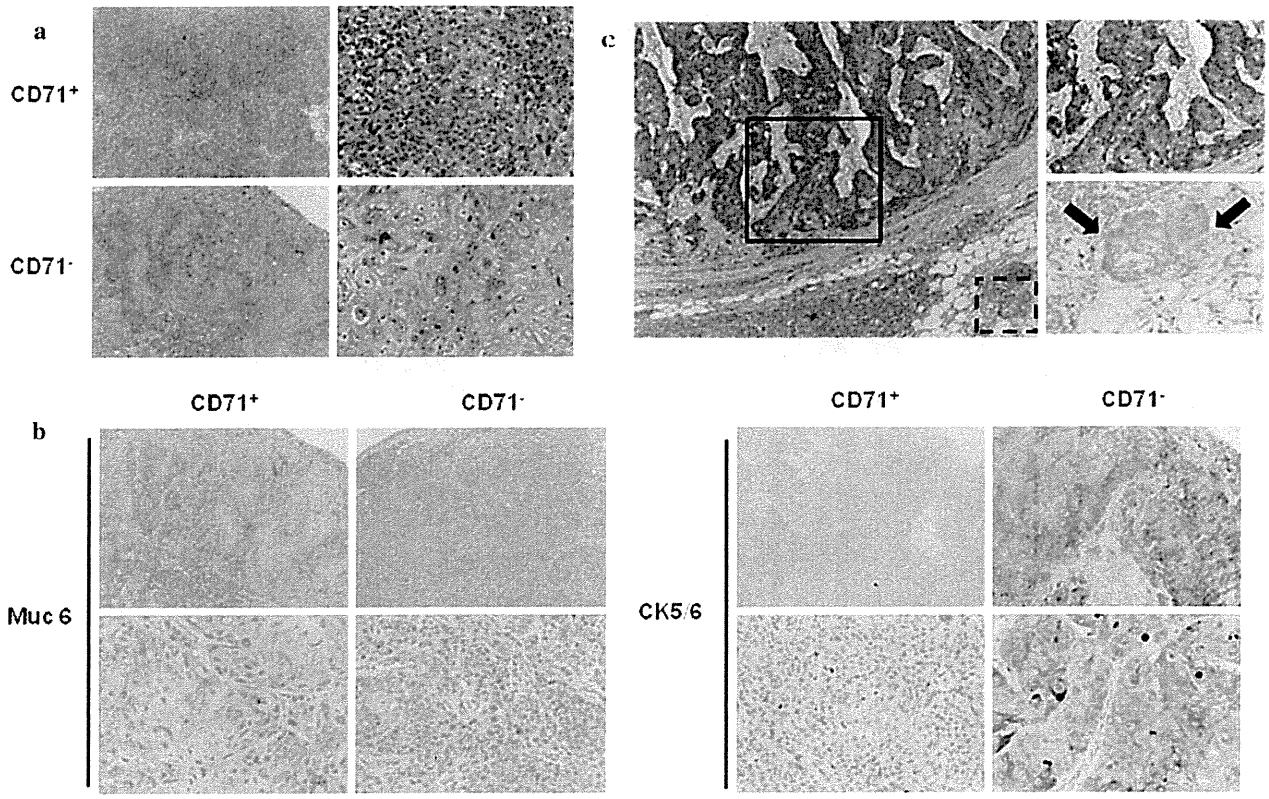

FIG. 4 CD71$^-$ cell fraction shows multipotency and exists in the invasive front of cancer foci: **a** Hematoxylin and eosin stain of tumor sections derived from isolated CD71$^-$ and CD71$^+$ cell fractions (*left*, ×10; *right*, ×20). **b** Immunohistochemical stains of tumor sections derived from isolated CD71$^-$ and CD71$^+$ cell fractions with anti-human MUC6 and anti-human CK 5/6 antibodies. Each of the *upper columns* shows the lower magnification (×10), and each *lower column* shows the higher magnification (×20). **c** Immunohistochemical stains with anti-human CD71 from a human gastric adenosquamous cancer specimen. The *left panel* shows the lower magnification (×10), and the *upper right panel* shows a higher magnification (×20) of the *solid square* in the *left panel*. The *lower right panel* shows a higher magnification (×20) of the invasive front of the cancer foci seen in the *dotted square* in the *left panel*

DISCUSSION

The significance of CSCs has become apparent over the past decade since the discovery of their importance in hematological malignancy.[19] CSCs are believed to play a key role in tumor relapse and metastasis. Increased knowledge of this role is expected to bring advances in cancer therapy, which has been limited until date.

In the present study, we identified the CD71$^-$ cell fraction as a potential multidifferentiation and high-tumorigenicity fraction in MKN-1 cells, which are a known cell line of gastric adenosquamous carcinoma. The CD71 transferrin receptor is a carrier protein that transports iron into the cell and maintains cellular iron homeostasis. Various stem cells have been reported to be CD71 diminished or negative, including hematopoietic, keratinocyte, and hair follicle bulge stem cells.[20–24] Malignant leukemic stem cells are also reported to be CD71$^-$.[25–28]

Multipotency is one of the important characters proving the stemness of CSCs. A marker that is useful for identifying a multipotential cell population will be a CSC marker. We studied CSCs using the MKN-1 cell line, a cell line derived from a very rare variant of adenosquamous carcinoma. CD44 and SP cells have been reported to be candidate markers of gastric cancer CSCs.[6,7] However, to the best of our knowledge, there has been no report that shows or identifies markers closely related to a multidifferentiation fraction. In the present study, staining with anti-MUC6, a differentiation marker for adenocarcinoma, and anti-CK 5/6, a differentiation marker for the squamous cell lineage, revealed that only tumors derived from CD71$^-$ cells contained MUC6- and CK 5/6-positive cells. This finding suggests the bilateral differentiation potential of CD71$^-$ cells into adenocarcinoma and squamous cell carcinoma. Histologically, the epithelial surface of the skin and esophagus are lined with squamous cells. As with keratinocyte stem cells, esophageal stem cells are reported to be CD71$^-$.[22,23,29,30] Although these reports are from studies of normal squamous stem cells, the fact that a squamous cell lineage can be derived from the CD71$^-$ cell

fraction may be relevant in the context of cancer. It is important to determine whether the squamous cell carcinoma and adenocarcinoma lineages can appear from a single cell.

The slow growth of CSCs partially contributes to their anticancer agent resistance and cancer recurrence after chemotherapy.[31] In leukemia, it has been reported that quiescent (existing in the G0 phase) leukemic CSCs survive after treatment with the common anticancer agent 5-FU.[32,33] It is also known that quiescent leukemic CSCs are $CD71^-$, and CD71 expression is closely related to cell cycle status as CD71 is expressed mainly in proliferative cells.[27,34] In the present study, $CD71^-$ cells were enriched after 5-FU treatment and accumulated during the G0/G1 cell cycle phase. These findings are compatible with previous studies of leukemic CSCs and suggest that the $CD71^-$ cell fraction survives after treatment with anticancer agents and contributes to cancer regrowth and recurrence.

In limiting dilution and serial transplantation assays, the $CD71^-$ cell fraction showed a comparatively higher ability to form tumors than the $CD71^+$ cell fraction. Although data from the limiting dilution and serial transplantation experiments were not as clear as we expected, at least in the $CD71^-$ fraction, there was a characteristic cell population that showed self-renewal and bipotentiality. In liver cancer, both semiquiescent CSCs and proliferating progenitor-like cells show tumorigenicity.[35] As with liver cancer, there may be a cancer hierarchy in gastric adenosquamous carcinoma. Given that the $CD71^-$ fraction has relatively high tumorigenic activity and only the $CD71^-$ fraction displays bipotentiality, there may be at least two cellular fractions in $CD71^-$ cells: semiquiescent bipotential CSCs and proliferating progenitor cells. Furthermore, when the mature cancer cell, without tumorigenicity, is in the G1 cell cycle phase, these cells may also be $CD71^-$. Thus, CD71 could be used to isolate a bipotential CSC-enriched population but is not sufficient to isolate a definitive CSC population by itself. Additional markers are required to identify and isolate definitive CSCs.

In the present study, $CD71^-$ cells showed high migratory and invasive ability. These data were also supported by a 3D culture of $CD71^-$ cells, which revealed that $CD71^-$ cells had globular features. Immunohistochemical analysis of clinical gastric adenosquamous carcinoma revealed that the invasive front of the cancer foci was negative for CD71. It is known that gastric adenosquamous carcinoma is highly metastatic in early stages and has poor prognosis.[36] $CD71^-$ cells have high potential for metastasis and produce cells of the squamous carcinoma phenotype, and metastatic lesions of adenosquamous carcinoma are mainly replaced by squamous carcinoma.[36] These observations suggest that $CD71^-$ cells are migratory and invasive, leading to metastasis in the early stages of cancer and later differentiating to squamous cell carcinoma and adenocarcinoma. Unfortunately, no metastatic lesions were observed in the $CD71^-$ or $CD71^+$ fraction when these were subcutaneously inoculated into mice. To assess the metastatic ability of these fractions physiologically and biologically in order to determine their clinical features, it may be better to inoculate cells into the subserosa of the stomach.

The present study, which was based on a cancer cell line, suggests that $CD71^-$ cells have important roles in cancer development; it has furthered our understanding of the cancer cell hierarchy. It is now necessary to confirm the roles of $CD71^-$ cells in the most common gastric cancer, adenocarcinoma.

ACKNOWLEDGMENT We thank T. Shimooka for excellent technical assistance. This work was supported in part by a grant from Core Research for Evolutional Science and Technology, and grants-in-aid for scientific research on priority areas (20012039) and for scientific research (S) (21229015) from the Ministry of Education, Culture, Sports, Science, and Technology, Japan.

DISCLOSURE There is no conflict of interest.

REFERENCES

1. Reya T, Morrison SJ, Clarke MF, Weissman IL. Stem cells, cancer, and cancer stem cells. *Nature.* 2001;414(6859):105–11.
2. Pardal R, Clarke MF, Morrison SJ. Applying the principles of stem-cell biology to cancer. *Nat Rev Cancer.* 2003;3(12):895–902.
3. Beachy PA, Karhadkar SS, Berman DM. Tissue repair and stem cell renewal in carcinogenesis. *Nature.* 2004;432(7015):324–31.
4. Polyak K, Hahn WC. Roots and stems: stem cells in cancer. *Nat Med.* 2006;12(3):296–300.
5. Tanaka K, Kiyohara Y, Kubo M, et al. Secular trends in the incidence, mortality, and survival rate of gastric cancer in a general Japanese population: the Hisayama study. *Cancer Causes Control.* 2005;16(5):573–8.
6. Takaishi S, Okumura T, Tu S, et al. Identification of gastric cancer stem cells using the cell surface marker CD44. *Stem Cells.* 2009;27(5):1006–20.
7. Nishii T, Yashiro M, Shinto O, Sawada T, Ohira M, Hirakawa K. Cancer stem cell-like SP cells have a high adhesion ability to the peritoneum in gastric carcinoma. *Cancer Sci.* 2009;100(8):1397–402.
8. Boku N. Chemotherapy for metastatic gastric cancer in Japan. *Int J Clin Oncol.* 2008;13(6):483–7.
9. Boku N. Gastrointestinal Oncology Study Group of Japan Clinical Oncology Group. Chemotherapy for metastatic disease: review from JCOG trials. *Int J Clin Oncol.* 2008;13(3):196–200.
10. Al-Hajj M, Wicha MS, Benito-Hernandez A, Morrison SJ, Clarke MF. Prospective identification of tumorigenic breast cancer cells. *Proc Natl Acad Sci USA.* 2003;100(7):3983–8.
11. Singh SK, Hawkins C, Clarke ID, et al. Identification of human brain tumour initiating cells. *Nature.* 2004;432(7015):396–401.
12. O'Brien CA, Pollett A, Gallinger S, Dick JE. A human colon cancer cell capable of initiating tumour growth in immunodeficient mice. *Nature.* 2007;445(7123):106–10.

13. Ricci-Vitiani L, Lombardi DG, Pilozzi E, et al. Identification and expansion of human colon-cancer-initiating cells. *Nature.* 2007;445(7123):111–5.
14. Joshi PA, Jackson HW, Beristain AG, et al. Progesterone induces adult mammary stem cell expansion. *Nature.* 2010;465(7299): 803–7.
15. Lathia JD, Gallagher J, Heddleston JM, et al. Integrin alpha 6 regulates glioblastoma stem cells. *Cell Stem Cell.* 2010;6(5):421–32.
16. Arai F, Hirao A, Ohmura M, et al. Tie2/angiopoietin-1 signaling regulates hematopoietic stem cell quiescence in the bone marrow niche. *Cell.* 2004;118(2):149–61.
17. Guan Y, Gerhard B, Hogge DE. Detection, isolation, and stimulation of quiescent primitive leukemic progenitor cells from patients with acute myeloid leukemia (AML). *Blood.* 2003; 101(8):3142–9.
18. Holyoake T, Jiang X, Eaves C, Eaves A. Isolation of a highly quiescent subpopulation of primitive leukemic cells in chronic myeloid leukemia. *Blood.* 1999;94(6):2056–64.
19. Lapidot T, Sirard C, Vormoor J, et al. A cell initiating human acute myeloid leukaemia after transplantation into SCID mice. *Nature.* 1994;367(6464):645–8.
20. Hogge DE, Lansdorp PM, Reid D, Gerhard B, Eaves CJ. Enhanced detection, maintenance, and differentiation of primitive human hematopoietic cells in cultures containing murine fibroblasts engineered to produce human steel factor, interleukin-3, and granulocyte colony-stimulating factor. *Blood.* 1996;88(10): 3765–73.
21. Yang G, Hisha H, Cui Y, et al. A new assay method for late CFU-S formation and long-term reconstituting activity using a small number of pluripotent hemopoietic stem cells. *Stem Cells.* 2002;20(3):241–8.
22. Tani H, Morris RJ, Kaur P. Enrichment for murine keratinocyte stem cells based on cell surface phenotype. *Proc Natl Acad Sci USA.* 2000;97(20):10960–5.
23. Calenic B, Ishkitiev N, Yaegaki K, et al. Magnetic separation and characterization of keratinocyte stem cells from human gingiva. *J Periodontal Res.* 2010;45(6):703–8.
24. Ohyama M, Terunuma A, Tock CL, et al. Characterization and isolation of stem cell-enriched human hair follicle bulge cells. *J Clin Invest.* 2006;116(1):249–60.
25. Yamazaki J, Mizukami T, Takizawa K, et al. Identification of cancer stem cells in a Tax-transgenic (Tax-Tg) mouse model of adult T-cell leukemia/lymphoma. *Blood.* 2009;114(13):2709–20.
26. Yalcintepe L, Frankel AE, Hogge DE. Expression of interleukin-3 receptor subunits on defined subpopulations of acute myeloid leukemia blasts predicts the cytotoxicity of diphtheria toxin interleukin-3 fusion protein against malignant progenitors that engraft in immunodeficient mice. *Blood.* 2006;108(10):3530–7.
27. Holyoake TL, Jiang X, Jorgensen HG, et al. Primitive quiescent leukemic cells from patients with chronic myeloid leukemia spontaneously initiate factor-independent growth in vitro in association with up-regulation of expression of interleukin-3. *Blood.* 2001;97(3):720–8.
28. Blair A, Hogge DE, Sutherland HJ. Most acute myeloid leukemia progenitor cells with long-term proliferative ability in vitro and in vivo have the phenotype CD34(+)/CD71(−)/HLA-DR−. *Blood.* 1998;92(11):4325–35.
29. Kalabis J, Oyama K, Okawa T, et al. A subpopulation of mouse esophageal basal cells has properties of stem cells with the capacity for self-renewal and lineage specification. *Clin Invest.* 2008;118(12):3860–9.
30. Croagh D, Phillips WA, Redvers R, Thomas RJ, Kaur P. Identification of candidate murine esophageal stem cells using a combination of cell kinetic studies and cell surface markers. *Stem Cells.* 2007;25(2):313–8.
31. Meng S, Tripathy D, Frenkel EP, et al. Circulating tumor cells in patients with breast cancer dormancy. *Clin Cancer Res.* 2004;10(24):8152–62.
32. Terpstra W, Ploemacher RE, Prins A, et al. Fluorouracil selectively spares acute myeloid leukemia cells with long-term growth abilities in immunodeficient mice and in culture. *Blood.* 1996;88(6):1944–50.
33. Chung SW, Chen H, Wong PM. Activation of quiescent ABL-transduced hemopoietic stem cells. *Oncogene.* 1996;13(11): 2397–405.
34. Sutherland R, Delia D, Schneider C, Newman R, Kemshead J, Greaves M. Ubiquitous cell-surface glycoprotein on tumor cells is proliferation-associated receptor for transferrin. *Proc Natl Acad Sci USA.* 1981;78(7):4515–9.
35. Haraguchi N, Ishii H, Mimori K, et al. CD13 is a therapeutic target in human liver cancer stem cells. *J Clin Invest.* 2010; 120(9):3326–39.
36. Yoshida K, Manabe T, Tsunoda T, Kimoto M, Tadaoka Y, Shimizu M. Early gastric cancer of adenosquamous carcinoma type: report of a case and review of literature. *Jpn J Clin Oncol.* 1996;26(4):252–7.

American Journal of Transplantation 2012; 12: 102–114
Wiley Periodicals Inc.

doi: 10.1111/j.1600-6143.2011.03771.x

Rapamycin Causes Upregulation of Autophagy and Impairs Islets Function Both *In Vitro* and *In Vivo*

M. Tanemura[a,*], Y. Ohmura[a], T. Deguchi[a], T. Machida[a], R. Tsukamoto[a], H. Wada[a], S. Kobayashi[a], S. Marubashi[a], H. Eguchi[a], T. Ito[b], H. Nagano[a], M. Mori[a] and Y. Doki[a]

Departments of [a]Gastroenterological Surgery and [b]Complementary and Alternative Medicine, Osaka University Graduate School of Medicine, Osaka, Japan
**Corresponding author: Masahiro Tanemura, mtanemura@gesurg.med.osaka-u.ac.jp*

Autophagy is a lysosomal degradation process of redundant or faulty cell components in normal cells. However, certain diseases are associated with dysfunctional autophagy. Rapamycin, a major immunosuppressant used in islet transplantation, is an inhibitor of mammalian target of rapamycin and is known to cause induction of autophagy. The objective of this study was to evaluate the *in vitro* and *in vivo* effects of rapamycin on pancreatic β cells. Rapamycin induced upregulation of autophagy in both cultured isolated islets and pancreatic β cells of green fluorescent protein–microtubule-associated protein 1 light chain 3 transgenic mice. Rapamycin reduced the viability of isolated β cells and down-regulated their insulin function, both *in vitro* and *in vivo*. In addition, rapamycin increased the percentages of apoptotic β cells and dead cells in both isolated and *in vivo* intact islets. Treatment with 3-methyladenine, an inhibitor of autophagy, abrogated the effects of rapamycin and restored β-cell function in both *in vitro* experiments and animal experiments. We conclude that rapamycin-induced islet dysfunction is mediated through upregulation of autophagy, with associated downregulation of insulin production and apoptosis of β cells. The results also showed that the use of an autophagy inhibitor abrogated these effects and promoted islet function and survival. The study findings suggest that targeting the autophagy pathway could be beneficial in promoting islet graft survival after transplantation.

Key words: Autophagy, islet transplantation, LC3, rapamycin, transgenic mice

Abbreviations: Atg gene, autophagy related gene; BSA, bovine serum albumin; FKBP-12, 12-kDa FK506-binding protein; GFP, green fluorescent protein; GAPDH, glyceraldehyde-3-phosphate; LC3, microtubule-associated protein 1 light chain 3; mTOR, mammalian target of rapamycin; PBS, phosphate-buffered saline; TUNEL, terminal deoxynucleotidyl transferase-mediated dUTP nick-end labeling; SD, standard deviation.

Received 18 March 2011, revised 22 August 2011 and accepted for publication 22 August 2011

Introduction

Autophagy, i.e. "self-eating," is an intracellular degradation system designed for degradation of cytoplasmic proteins and dysfunctional organelles after their sequestration in the autophagosome. To date, only microtubule-associated protein1 light chain 3 (LC3), a mammalian homolog of yeast autophagy related gene8 (Atg8), is known to exist in the autophagosomes, and therefore this protein serves as a marker for autophagosomes (1–3). The process is tightly regulated and plays an important role in cell growth, development and homeostasis, where it helps to maintain a balance between the synthesis, degradation and subsequent recycling of cellular components (1–3). Autophagy is induced dynamically by nutrient depletion to provide necessary amino acids within cells, thus helping them adapt to starvation (4). The physiological role of autophagy has been studied in various organisms and current knowledge indicates that autophagy is involved not only in adaptation to starvation but also in the quality control of intracellular proteins and organelles, to maintain cell functions, development, growth, clearance of intracellular microbes, antigen presentation and protection against disease (5–11). Thus, autophagy functions as a cell-protective mechanism and is up-regulated when cells are preparing to rid themselves of damaging cytoplasmic components, for example, during infection or protein aggregate accumulation (12).

Rapamycin is a macrolide fungicide with immunosuppressant properties that bear molecular structural similarities to the calcineurin inhibitor, tacrolimus (13). However, the mechanism of action of rapamycin is distinct from that of calcineurin inhibitor, such as cyclosporine and tacrolimus. Rapamycin binds to its intracellular receptor, the immunophilin 12-kDa FK506-binding protein (FKBP-12) and the rapamycin-FKBP-12 complex binds to and inhibits the mammalian target of rapamycin (mTOR; Ref. 14). Inhibition of mTOR leads to arrest of the cell cycle at the G1 to S phase and thus, blockade of growth-factor-driven proliferation of not only activated T cells, which constitute the basis of its immunosuppressive action, but also

other hematopoietic and nonhematopoietic cells (14,15). The mTOR is ubiquitously expressed in various cell types and functionally is a serine/threonine protein kinase that regulates important cellular process, including growth, proliferation, motility, survival, protein synthesis and transcription (16). Furthermore, activation of mTOR leads to inhibition of autophagy in cells ranging from yeast to human (17). Based on the above background, it is conceivable that the inhibitory action of rapamycin on mTOR activity induces autophagy in pancreatic islets.

Islet transplantation was recently advanced by the publication of the results of the Edmonton Protocol of immunosuppressive regimen, leading to insulin independence at 1 year in 90% of patients treated with type 1 diabetes (18–21). Accordingly, rapamycin has become a part of the standard treatment in islet transplantation. Its effectiveness in preventing allorejection and autoimmunity and promoting the survival of regulatory T lymphocytes has contributed to widespread use (22–24). However, recent reports described gradual deterioration of the metabolic profile and the need for reintroduction of exogenous insulin; only 10% of islet recipients maintained insulin independence at 5 years (21,25,26). Although the cause of the decline in insulin independence rates after islet transplantation remains obscure, the decline may reflect toxicity associated with long-term use of immunosuppressive drugs on islet β cells.

The effects of calcineurin inhibitors on islet function and proliferation have been recognized (27,28), although increasing data suggest that rapamycin alone or in combination with tacrolimus could impair islet cell function and survival (29–31). In addition, the antiangiogenic and antiproliferative properties of rapamycin could also prevent vascularization of transplanted islets, with a resultant reduction of posttransplantation engrafted and surviving islet mass (32–34).

Although it has been reported that β cells of ZDF rats (a rodent model of type 2 diabetes) contain a significant number of autophagic vacuoles (35), there is little information on the physiopathological roles of autophagy in the islets, and no causal link has been reported between autophagy and pathogenesis of diabetes. The aims of this study were to evaluate the *in vitro* and *in vivo* effects of rapamycin on pancreatic β cells, including induction of autophagy, cell viability and insulin secretory function, because these factors may contribute to progressive dysfunction of islet grafts in recipients.

Materials and Methods

In vitro *autophagy induction assay and islet viability assay*

Thirty cells from fresh mice islets, obtained from either C57BL/6 mice or green fluorescent protein (GFP)–LC3 transgenic mice were seeded in a 96-well culture plate and cultured for either 24 or 48 h with complete culture medium containing 1 or 10 ng/mL of rapamycin. In the first step, treated islets that were isolated from transgenic mice were observed by fluorescence microscopy to detect GFP signals, which is an accurate marker of induction of autophagy (36). Subsequently, islet viability was evaluated after 24 h treatment by monitoring metabolic activity with the colorimetric methyl tetrazolium salt (MTS) assay using the Cell Titer 96 Aqueous One reagent (Promega, Madison, WI, USA; Ref. 37). The colorimetric reagent was added to each well of the plate and incubated for 2 h, and the absorbance values read at 490 nm.

To further determine the change in islet viability before/after rapamycin treatment, fluorescence labeling was performed using tetramethyl rhodamine ethyl ester (TMRE; Molecular Probes, Eugene, OR, USA) and 7-amino actinomycin D (7-AAD; Molecular Probes; Refs. 38,39). Islets treated or untreated with rapamycin were dissociated into single cell suspensions, using Accutase (Innovative Cell Technologies Inc, San Diego, CA, USA). The dispersed cell suspensions were stained with Newport Green PDX acetoxymethylether (Molecular Probes), for identification of β cells (38). The single islet cell suspensions were incubated with 100 ng/mL TMRE for 30 min at 37°C in phosphate-buffered saline (PBS) without Ca^{2+} and Mg^{2+}. This dye selectively binds to the mitochondrial membrane allowing the assessment of cells with functional mitochondria, and therefore is a good marker for cell viability. Furthermore, cells were stained with 7-AAD that binds to DNA when cell membrane permeability is altered after cell death. Stained cells were analyzed by FACSCalibur flow cytometer (BD Immunocytometry, San Jose, CA, USA). In addition, improvement in islet viability was assessed by either MTS assay, TMRE or 7-AAD staining based on the results of autophagic signal blocking. Islet viability assays were performed with the addition of 10 mM of 3-methyladenine (3-MA).

Glucose-stimulated insulin release and stimulation index (SI)

To determine the changes in the endocrinological potency of rapamycin-treated islets, static glucose challenge was performed with or without 1 or 10 ng/mL of rapamycin. After overnight culture with or without rapamycin, 100 IEQ of treated islets were incubated with either 2.8 or 20 mM of glucose in culture medium for 2 h at 37°C to stimulate insulin release. The supernatants were collected and stored at −80°C for insulin assessment by enzyme-linked immunosorbent assay (ELISA; Mercodia Inc., Uppsala, Sweden; Refs. 38–40). Glucose-stimulated insulin release was expressed as the SI, calculated as the ratio of insulin released during exposure to high glucose (20 mM) over that released during low glucose incubation (2.8 mM). To determine the *in vitro* islet potency with regard to autophagic signal blocking, static incubation was also performed with the addition of 10 mM of 3-MA.

In vivo *studies using GFP-LC3 transgenic mice*

To study the effects of starvation, transgenic mice were provided with drinking water *ad libitum*, but were deprived of food for 24 h (10 a.m.–10 a.m.; Ref. 36). The starved transgenic mice were sacrificed and the pancreas, brain and muscle tissues were recovered. This was followed by preparation of the tissues for fluorescence microscopy. Furthermore, to demonstrate *in vivo* 3-MA-induced blocking of autophagy, mice were injected intraperitoneally (i.p.) with 10 mM of 3-MA for 2 weeks, followed by starvation for 24 h.

To assess the *in vivo* effects of rapamycin on islets from GFP-LC3 transgenic mice, mice were randomly separated into three experimental groups, no treatment group (i.e. control group; n = 25), rapamycin-treated group (n = 25) and the combination treatment group (n = 25) treated with both rapamycin and 3-MA. Rapamycin treatment consisted of daily i.p. injection of 0.2 mg/kg rapamycin and combined treatment consisted of daily i.p. injection of 0.2 mg/kg rapamycin combined with 10 mM of 3-MA. These treatments continued for 1, 2, 3, 4 or 5 weeks (n = 5 mice, each). The rapamycin-treated transgenic mice were sacrificed, the pancreas was removed and

processed for fluorescence and immunofluorescence microscopy. During rapamycin treatment, nonfasting blood glucose level was monitored daily using samples obtained from the tail vein. To further determine the effects of rapamycin on glucose tolerance, intraperitoneal glucose tolerance test (IPGTT) was conducted before and at days 14 and 28 after treatment (41). In this test, mice were fasted for 6 h and then injected intraperitoneally with 2 g glucose in saline/kg body weight. Blood glucose levels were measured for 2 h at 30 min intervals. Moreover, to detect the change in insulin secretion after *in vivo* rapamycin treatment, plasma insulin levels were also measured by ELISA before and after the treatment (at days 0, 7, 14, 21, 28 and 35, n = 5 mice, each group).

Fluorescence microscopy and immunofluorescence microscopy

Pancreatic tissue samples for GFP examination were prepared as follows. To prevent artificial induction of autophagy during sample preparation, mice were anesthetized by diethyl ether and immediately fixed by transcardial perfusion through the left ventricle with 4% paraformaldehyde dissolved in 0.1 M Na-phosphate buffer (pH 7.4). Subsequently, the pancreas was removed and further fixed with the same fixative for another 4 h at room temperature, followed by treatment with 5% sucrose in PBS for 2 h and then with 15% sucrose solution for 4 h, finally with 30% sucrose solution overnight. Pancreatic tissue samples were embedded in Tissue-Tek OCT compound (Sakura Finetechnical Co., Tokyo, Japan) and stored at −80°C. The tissue samples were sectioned at 7 μm thickness with a cryostat, air-dried for 30 min at room temperature and then stored at −80°C until use. Fluorescence signals were analyzed by Biozero fluorescence microscopy (Keyence, Osaka, Japan) by measuring green fluorescence (excitation, 488 nm; emission, 530 nm).

For general histological examination, cryosections were stained with hematoxylin and eosin. Furthermore, for immunofluorescence microscopy, cryosections were prepared as described earlier. After rinsing with water for 5 min, the sections were blocked with 4% bovine serum albumin (BSA)–PBS for 10 min at room temperature. Subsequently, these sections were incubated with rabbit polyclonal anti-mouse insulin Ab (SC-9168; Santa Cruz Biotechnology, Santa Cruz, CA, USA) overnight at 4°C diluted in 1% BSA-TBS-Tween-20 (0.05% w/v), followed by incubation with Alexa fluor555 goat anti-mouse IgG (H+L) Ab (A21429; 1:1000 dilution; Invitrogen, Carlsbad, CA, USA) for 30 min at room temperature. Fluorescence signals were observed by Biozero fluorescence microscopy (Keyence). The fluorescence intensities of insulin and GFP-LC3 in treated islets were quantified using Fluor-Chem image analyzer (Bio-Rad Laboratories Inc., Hercules, CA, USA) and expressed in arbitrary units. The mean fluorescence intensities of insulin and GFP, expressed as mean ± standard deviation (SD), were determined in islets of five rapamycin-treated mice. To identify apoptotic β cells in the pancreas of mice, islet sections were stained with terminal deoxynucleotidyl transferase-mediated dUTP nick-end labeling (TUNEL) using Tumor TACS™ *In Situ* Apoptosis Detection Kit (catalog# 4815–30-K, Trevigen, Gaithersburg, MD, USA) following the instructions provided by the manufacturer.

Statistical analysis

Data were expressed as mean ± SD and analyzed using Excel for Windows software. Two samples were compared with the Student's *t*-test. The p values <0.05 denoted the presence of statistical significance.

Details of the mice used in these experiments, islet isolation to assess the effects of rapamycin treatment *in vitro* and western blot analysis are presented in the Supplementary Materials and Methods in the on line version of the journal.

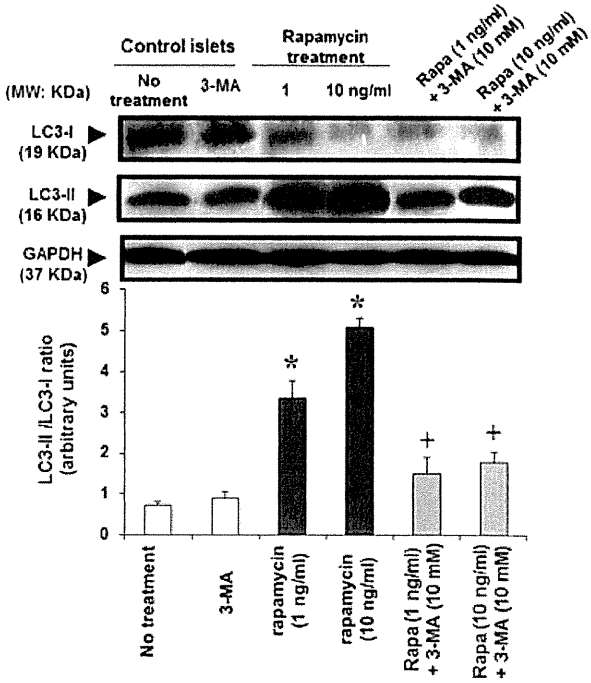

Figure 1: Changes in LC3-I and LC3-II protein expression levels in rapamycin-treated islets. LC3-I and LC3-II protein expression level were examined by western blot analysis. Protein samples extracted from either untreated islets, rapamycin-treated or rapamycin + 3-MA-treated islets were subjected to 15% SDS/PAGE and transferred onto PVDF membrane. Representative photographs are shown, together with mouse GAPDH levels as an internal control. Quantification of the intensity of the immunoreactive bands of both LC3-I and LC3-II, expressed in arbitrary units, was carried out using NIH Image J software. Results of densitometric analysis of immunoblots of LC3 in islets were expressed as the ratio of LC3-II to LC3-I. Data are mean ± SD of three independent experiments. *$p < 0.05$, versus control islet; $^{+}p < 0.05$, versus rapamycin-treated islets.

Results

In vitro *overinduction of autophagy in pancreatic islets by rapamycin*

Control islets, including untreated islets and 3-MA-treated islets, showed similar levels of endogenous expression of LC3-II protein (Figure 1). Islets treated with 1 or 10 ng/mL of rapamycin showed the highest expression of LC3-II protein. The conversion of LC3-I (cytosolic form) to LC3-II (membrane-bound lapidated form) was detected by immunoblotting. The amounts of LC3-II protein were three- to fivefold higher in 1 and 10 ng/mL rapamycin-treated islets, respectively, as assessed by the LC3-II/LC3-I ratio (Figure 1). The rapamycin-induced increase in LC3-II level suggests increased autophagy flux. Quantification of LC3-II band intensities showed that blockade of autophagy by 3-MA prevented the accumulation of LC3-II protein in islets treated with 1 or 10 ng/mL of rapamycin. With regard

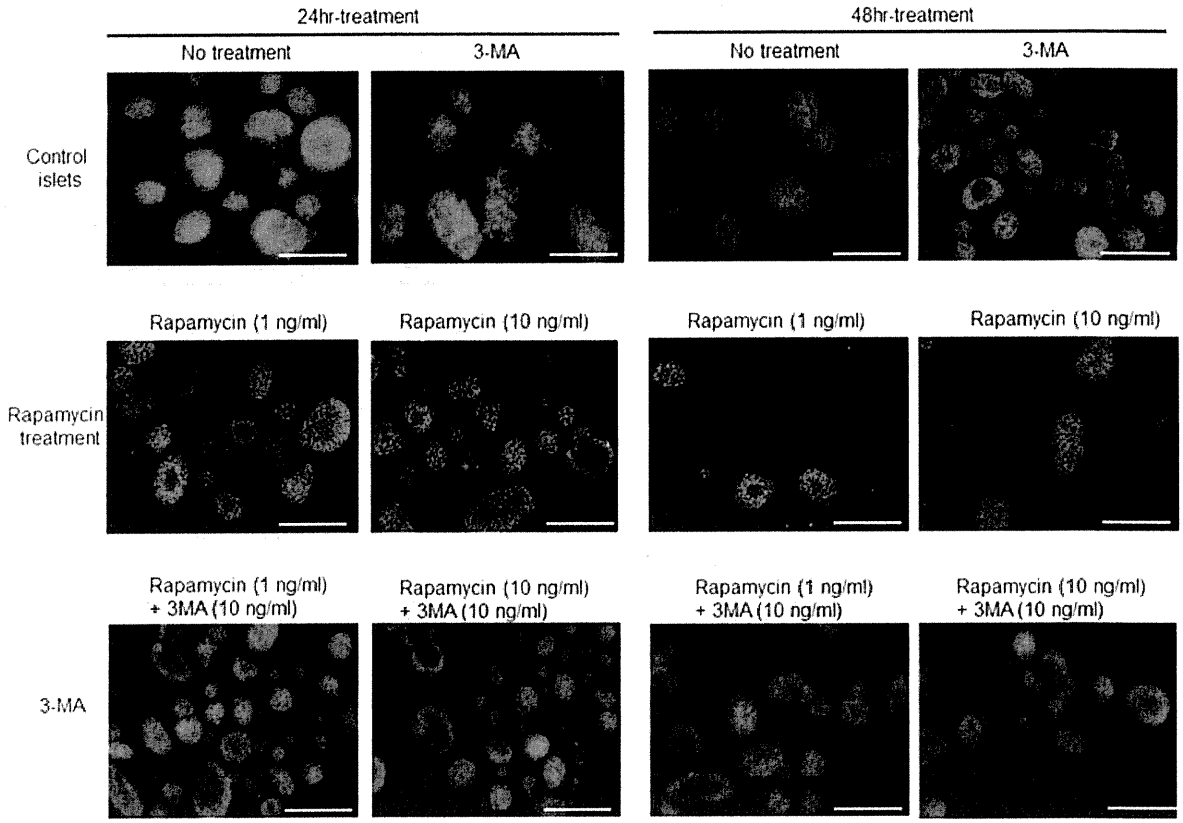

Figure 2: *In vitro* overinduction of autophagy in response to rapamycin treatment. Fresh islets samples were prepared from GFP-LC3 transgenic mice, and then incubated for either 24 or 48 h in the absence or presence of rapamycin. In 3-MA blocking, fresh islets were incubated in the presence of both rapamycin and 3-MA. After treatment, the GFP signal was detected by fluorescence microscopy. Bars = 100 μm.

to the conversion of LC3-I to LC3-II, the LC3-II/LC3-I ratio was significantly reduced in islets treated with rapamycin-plus-10 mM 3-MA compared with that of islets treated with rapamycin alone (Figure 1).

As shown in the top panels of Figure 2, a diffuse GFP-LC3 signal was detected in the control islets, with few GFP puncture dots. After 24 h incubation with 1 or 10 ng/mL of rapamycin, the number of GFP-LC3 dots was markedly increased; most dots were detected as cup- or ring-shaped structures (left middle panels, Figure 2). These findings indicate overinduction of autophagy in rapamycin-treated islets. In contrast, the fluorescence level of GFP-LC3 signal in rapamycin-treated islets in the presence of 10 mM 3-MA was diffuse and returned to the basal level of autophagy in control islets (left bottom panels, Figure 2). After 48 h incubation with rapamycin, many large ring- or cup-shaped structures were identified by fluorescence microscopy (right middle panels, Figure 2). Furthermore, the fluorescence signals of GFP-LC3 in rapamycin-plus-3-MA-treated islets continued to show diffuse distribution and persisted at the basal level of autophagy seen in the control islets (right bottom panels, Figure 2). Taken together, the results indicate that the blocking effects of 3-MA were persistent rather than transient.

Rapamycin-related overinduction of autophagy in islet cells reduces islet viability

To examine the effect of overinduction of autophagy by rapamycin on islet viability, we performed MTS assay (Figure 3) and fluorescence labeling with TMRE and 7-AAD (Figure 4). Viability under treatment with 3-MA alone was similar to the control islets (Figure 3). Treatment with 1 and 10 ng/mL rapamycin resulted in approximately 43% and 51% reduction of viability, respectively (Figure 3). In contrast, 3-MA ameliorated the effect of rapamycin on islet viability (Figure 3).

To further determine the effect of rapamycin on islet viability, islet cells were stained with TMRE or 7-AAD and assessed by FACS analysis. 3-MA had no significant effect on islet viability (control, 80.5 ± 4.5%; 3-MA, 80.4 ± 5.5%) and the percentages of dead cells (i.e. 7-AAD-positive cells; control, 4.7 ± 3.5%; 3-MA, 3.9 ± 4.3%). Rapamycin significantly decreased the proportion of TMRE-positive cells

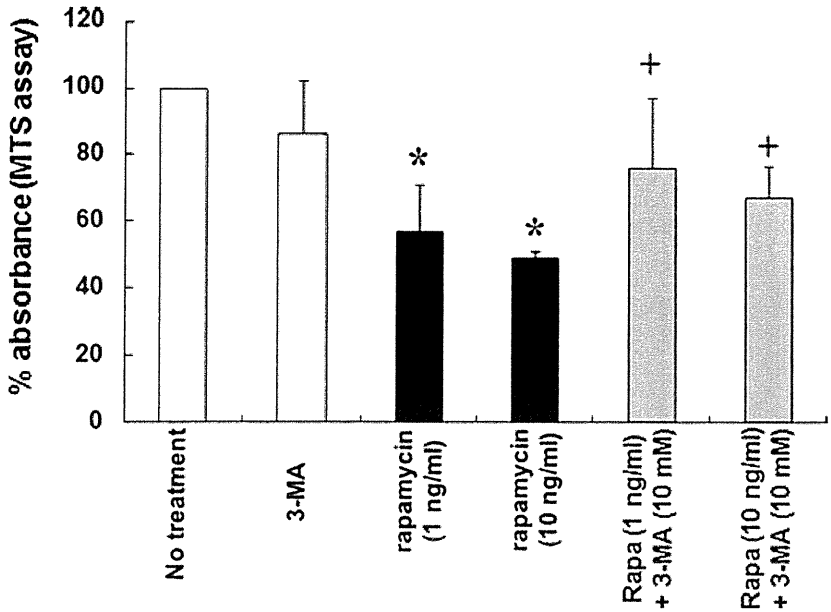

Figure 3: *In vitro* viability assessments of rapamycin-treated islet by MTS assay. Control islets, rapamycin-treated and rapamycin-3-MA-treated islets were assessed for islet viability. Data are mean ± SD of five independent islets preparations. The% absorbance of treated islets was expressed relative to absorbance of control islets, which was set at 100%. *$p < 0.05$, versus control islets; $^{+}p < 0.05$, versus rapamycin-treated islets.

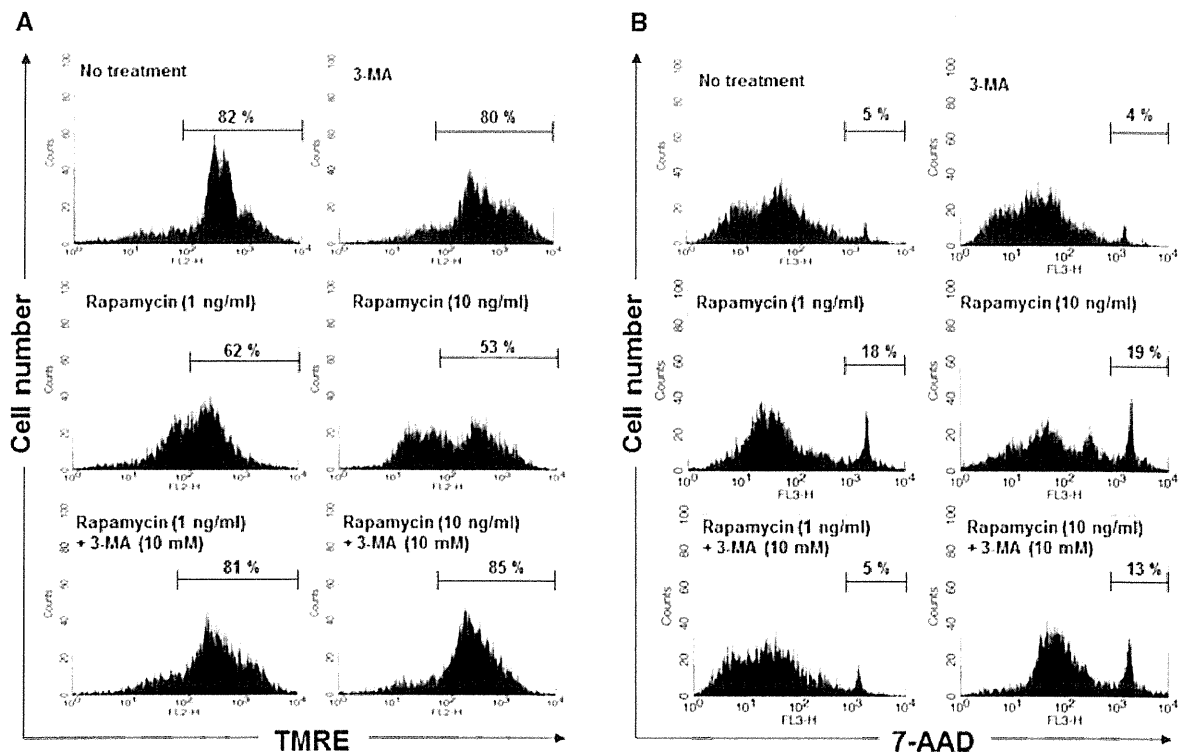

Figure 4: *In vitro* analysis of the cytotoxic effect of rapamycin and upregulation of autophagy. Islets were incubated with either 1 or 10 ng/mL of rapamycin for 24 h to overinduce autophagy. In blocking assay, islets were cultured with rapamycin in the presence of 10 mM 3-MA. After dispersion of mice islets into single cell suspensions, cells were stained with TMRE or 7-AAD. (A) Pancreatic β cells were analyzed for the relative percentage of apoptotic or nonapoptotic cells by TMRE. (B) Dead cells represented 7-AAD-positive cells. Data are representative of five independent experiments using different mice islets reparations.